



A computational approach to the powered Swing-By in the elliptic restricted problem

Alessandra F. S. Ferreira¹ · Rodolpho V. de Moraes¹ · Antônio F. B. A. Prado² · Othon C. Winter¹ · Denilson P. S. Santos³

Received: 14 July 2020 / Accepted: 24 February 2021
© The Brazilian Society of Mechanical Sciences and Engineering 2021

Abstract

This work performs a computational investigation of the energy variations given by a powered Swing-By maneuver realized in an elliptical system. It extends previous works by giving the freedom to choose the location and the direction of the thrust vector, aspects that were not considered before in the literature. Those variations are obtained numerically as a function of the parameters related to the thrust (magnitude, direction and location of the application) and the orbital parameters of the primaries (eccentricity and true anomaly). The maneuver is realized around the smaller primary, and the energy variations are measured with respect to the main body of the system. The initial orbit of the space vehicle is defined by its periapsis distance, angle and approach velocity with respect to the smaller primary. The study is applied to a system composed of two primaries that are in elliptic orbits around the center of mass of the system. The eccentricity is varied as a free parameter, to measure its effects. The results show that the best maneuvers apply the thrust at a point inside the sphere of influence of the secondary body, but not in the periapsis of the orbit. The best direction of the thrust is not aligned with the motion of the space vehicle. The techniques studied here are applied in situations where it is desired to increase the energy of the space vehicle. Empirical equations are obtained for the energy variations, based on the simulations made in the present paper. The numerical approach makes the results more accurate and not limited to particular regions of the eccentricity.

Keywords Astrodynamics · Close approach · Orbital maneuvers · Elliptical system · Energy variation

1 Introduction

The present paper makes an investigation of the energy variations given by a powered Swing-By maneuver (PSBM) realized in a system of primaries that are in elliptic orbits around the center of mass of the system and with free location and direction of application of the thrust. The maneuver is realized around the secondary body and the energy variations are measured with respect to the main body of the system.

The PSBM is a combination of a pure gravity Swing-By, which depends only on the gravity field of the celestial body and the geometry of the passage, with the application of an impulsive maneuver in the space vehicle at some point inside the sphere of influence of the body involved in the maneuver. Minovitch, in 1961 [1], made one of the first studies related to engineering applications of the pure gravity Swing-By maneuver. He showed the basic physics involved in this close approach maneuver when applied to trajectories of a space vehicle, and the possibility of using this technique

Technical Editor: Flávio Silvestre.

✉ Alessandra F. S. Ferreira
aleferrazzsilva@hotmail.com

Rodolpho V. de Moraes
rodolpho.vilhena@gmail.com

Antônio F. B. A. Prado
antonio.prado@inpe.br

Othon C. Winter
ocwinter@gmail.com

Denilson P. S. Santos
denilson.santos@unesp.br

¹ São Paulo State University - UNESP, Guaratinguetá, São Paulo 12516-410, Brazil

² National Institute of Space Research - INPE, São José dos Campos, São Paulo 12227-010, Brazil

³ São Paulo State University - UNESP, São João da Boa Vista, São Paulo 13876-750, Brazil

to send a space vehicle out of the Solar System with much smaller fuel consumption, when compared to maneuvers made exclusively based on propulsion systems [2, 3].

Looking for missions that already used this technique, Flandro, in 1966 [4], showed the detailed plan for the Voyager mission, which is a mission composed of two space vehicles that made a series of close approaches with several planets of the Solar System to gain energy for the trip. The calculations were made based on Minovitch [1], and it was possible to verify the efficiency of this maneuver in a grand tour of the Solar System. The Galileo mission also used passages by the planets of the Solar System to increase its energy, so helping the space vehicle to complete the goals of the mission [5, 6].

More recently, we had the missions Messenger and Bepi-Colombo, which are two missions directed to the planet Mercury [7–9]. Mercury has a very large eccentricity and close approach maneuvers around it cannot be accurately studied under the approach given by assuming a circular orbit for Mercury. Besides those real applications, several other studies about the Swing-By maneuver are available [10–17].

The use of the PSBM is an important option when the energy obtained from a pure gravity Swing-By maneuver is not enough to achieve the goals of the mission. The flexibility given to the geometry of the close approach can give larger energy variations for the space vehicle. Several goals are possible in this maneuver: to find the best geometry to get as much energy as possible from this maneuver to send a space vehicle somewhere; to approach the body close enough to be captured; or even to collide with its surface.

In this study, we develop an analysis to find the best geometries for the maneuver based on the variations of the parameters related to the thrust: α , which defines the thrust direction; θ , which defines the thrust location, and δV , the magnitude of the thrust; and the effects coming from the geometry of the primaries: e , the eccentricity of the orbits of the primaries, and ν , the true anomaly of the secondary body at the moment of the closest approach. It is known that the velocity of a celestial body in an elliptic orbit is not constant and, for a given semi-major axis, the distance between the primaries at the periapsis reduces with the eccentricity of the orbit. Therefore, there is an important influence of the eccentricity in the energy variations given by this maneuver.

The PSBM has been studied before for the circular case [18–23], and the results showed the benefits of this combined maneuver. As a natural sequence of studies, this paper extends those researches to systems where the primaries are in elliptical orbits. This is a point of interest from the academic point of view, to learn the effects of the eccentricity of the orbits of the primaries in this maneuver, as well as from the engineering side, because there are several systems with considerable eccentricity in the Solar System. Good

examples are Mars, which has an eccentricity of 0.093; and Mercury, with an eccentricity of 0.2056. Both of those planets have been considered many times for Swing-By maneuvers [24–27] and can benefit from the present computational study. In these cases, the effects of the maneuver are larger when we consider their eccentricities, as shown in [28] and [29].

An initial analytical and superficial study of this problem suggests that the best place to apply the thrust is during the closet approach, because it is the point of maximum velocity, which increases the energy transfer from the impulsive maneuver to the space vehicle. However, the literature shows that, for the circular case, this is not true, and some deviations in the direction of the thrust [19, 22] and in the point of its application [21, 23] can increase the energy gains of the maneuver. Ferreira et al. [22] made a study analyzing the gains and losses of energy of a space vehicle in a Swing-By maneuver when the thrust is applied in different directions. In 2017, Ferreira et al. [23] expanded this study, varying not only the direction, but also the thrust location. In this work, only the energy gains were analyzed. Recently, Ferreira et al. (2017b) [30] studied the best directions to apply the thrust, for an eccentric system, in the situations where the application point is in the periapsis of the orbit of the space vehicle around the secondary body.

To extend this line of research, the present paper studies the more complete case, where the thrust has freedom to be applied in any point inside the sphere of influence of the secondary body and in any direction, in an elliptical system. The simulations showed that to apply the thrust in a location different from the periapsis and in a direction that is not tangent to trajectory of the spacecraft is also more efficient when the primaries are in elliptical orbits. Compared to the circular problem studied before [19, 21–23, 31], substantial differences appear for eccentricities of the order of 0.1, near the value of the Sun–Mars system, and below the value for the Sun–Mercury system. The reason is based on the fact that, when the thrust is applied under different initial conditions, with variations in the parameters, the energy variations due to the gravitational part of the maneuver are also changed. Therefore, the best results can be found only by computational techniques, like the one used here. It happens because the orbit changes instantly, so the geometry of approach is different, including a new periapsis distance and a new approach angle, which changes the gravitational effects of the gravity part of the maneuver. So, the application of the thrust outside the periapsis can be more efficient in several conditions; as well as it generates a more flexible maneuver, which might attend several other constraints of the mission, not only to increase energy variations. This is shown in details for the circular case in [23], and the present paper extends this study for an elliptical system.

This research calculates energy variations for a system of primaries with sizes and masses similar to the Earth–Moon system, but generalizing the eccentricity of the orbit of the primaries to study the effects of this parameter. The direction and location of the impulse are free parameters in the maneuver, therefore they are used to maximize the energy gains. It is also possible to consider situations of losses of energy for the space vehicle, but it is necessary to make some specific considerations and this case will not be covered here.

In particular, the present research studies the effects of the magnitude of the thrust in the energy variations. A detailed analysis is also performed to show the importance of applying the thrust in a position different from the periapsis of the trajectory of the space vehicle around the smaller primary, an assumption that was made in most of the already cited literature.

Another point considered here is the development of empirical equations based on the results given by the computational simulations of energy variations. These equations can be useful to estimate energy variations without the need of extra simulations.

The computational approach gives more accurate results and does not limit the values for the variables involved, such as the eccentricity of the primaries and/or the magnitude of the thrust.

2 Powered Swing-By maneuvers (PSBM)

As already explained, the PSBM is a technique where the space vehicle approaches a celestial body and takes advantage of the gravity of this body to modify its trajectory, but this effect is combined with a thrust applied in the space vehicle by a propulsive system. It is a complex maneuver if compared to the “pure gravity Swing-By,” where the only forces acting in the motion of the space vehicle are the ones coming from the gravity fields of the celestial bodies involved.

In the present research, the thrust is applied in different locations of the trajectory of the space vehicle, but always inside the sphere of influence of the near celestial body. The present study also varies the direction and magnitude of the thrust with the goal of studying the effects of those parameters in the combined maneuver.

As done in [30], the dynamics of the system is based on the “Elliptical Restricted Three-Body Problem” [32–34]. The definition of the system follows the usual form used in the literature and the more massive body, called M_1 , is the primary body of the system. The secondary body is M_2 , the second largest in mass, and the space vehicle is M_3 , which

is assumed to have a negligible mass. M_1 and M_2 are moving in elliptical orbits around their center of mass, and M_3 performs the Swing-By around M_2 . In the situations studied in the present research, the movement is limited to the orbital plane of the primaries. The mass of M_1 is given by $1 - \mu$ in canonical units, with $\mu = \frac{m_2}{(m_1+m_2)}$ being the mass of the secondary body, also in canonical units. m_1 and m_2 are the masses of M_1 and M_2 , respectively, in metric units. The canonical units system (c.u.) is a system where the total mass of the system ($M = m_1 + m_2$) is one; the semi-major axis “ a ” of the orbit of the primaries is the unit of distance; the gravitational constant is also one; and the time unit is defined to make the orbital period of the primaries to be 2π . From basic celestial mechanics, it is known that the distance between M_1 and M_2 is given by $d = \frac{a(1-e^2)}{1+e \cos v}$, where e and v are the eccentricity of the orbit of M_2 and the true anomaly of M_2 , respectively.

In this way, the main objective of this research is to study the effects of different geometries and characteristics of the thrust in the variations of energy, in particular, to find the locations of the extreme variations. To make this search, the equations of motion (Eqs. 1 and 2) are integrated backward and forward in time, always starting at the periapsis and going until points that are very far from the secondary body. Because there is a large computational effort and the numerical integrations are relatively fast, we adopted this distance as half of the distance between the main bodies, which gives a large safety margin to guarantee the non-influence of M_2 . We do not adopt the sphere of influence (SOI) of the body, since the sphere of influence is an approximated way of measuring how far the body has influence, but in fact, the effect of the secondary body extends beyond this sphere of influence. Another reason to maintain this value is to keep consistency with other works available in the literature [19, 22, 23], since all of them that used this value, allowing more accurate comparisons and validations of the results. At those two distant points, the two-body energy space vehicle— M_1 before and after the maneuver are measured, which gives the information to calculate the variations of energy due to the close approach to M_2 .

For the numerical integrations, the initial conditions of the orbit of the space vehicle are obtained from the parameters that define the close approach trajectory [30]: r_p , the periapsis distance, which is the distance between M_2 and the periapsis of the orbit of the space vehicle around it; ψ , the approach angle, the angular distance between the line of the primaries and the line of periapsis; and $V_{\infty-}$, the velocity of approach of the space vehicle with respect to M_2 ; e and v , the eccentricity and the true anomaly of M_2 at the time of the closest approach of the space vehicle with M_2 . The equations of motion of the space vehicle are given by Eqs. (1–2) [32].

$$\ddot{x} = \frac{-(1 - \mu)(x - x_1)}{r_1^3} - \frac{\mu(x - x_2)}{r_2^3} \tag{1}$$

$$\ddot{y} = \frac{-(1 - \mu)(y - y_1)}{r_1^3} - \frac{\mu(y - y_2)}{r_2^3}. \tag{2}$$

In those equations, r_1 represents the distance between M_1 and the space vehicle; r_2 the distance between M_2 and the space vehicle; and (x_1, y_1) and (x_2, y_2) the positions of M_1 and M_2 , respectively.

Figure 1 shows the geometry of the maneuver. \vec{V}_- is the velocity of the space vehicle with respect to M_2 , at point Q , before the application of the thrust. \vec{V}_+ is the velocity of the space vehicle with respect to M_2 , also at the point Q , but after the application of the thrust. The velocity vector of M_2 relative to the primary body is denoted by \vec{V}_2 . $\delta\vec{V}$ is the thrust vector, with magnitude δV , and α is the angle that defines the direction of the thrust, measured with respect to the direction of the motion of the space vehicle. Its value is given from an initial guess, and some of its characteristics can be highlighted as follows: if $-90^\circ < \alpha < 90^\circ$, the space vehicle is accelerated by the impulsive part of the maneuver, because there is a component in the direction of motion; for $\alpha < -90^\circ$ or $\alpha > 90^\circ$, the thrust has a component opposite to the direction of the motion of the space vehicle, making a deceleration; if α is between -180° and 0° , the thrust has a component pointing to the secondary body and, if α is between 0° and 180° , the thrust has a component pointing opposite to the secondary body.

The gray continuous line represents the trajectory of the space vehicle before the thrust, which ends at the point Q , where the thrust is applied. The gray dashed line is the

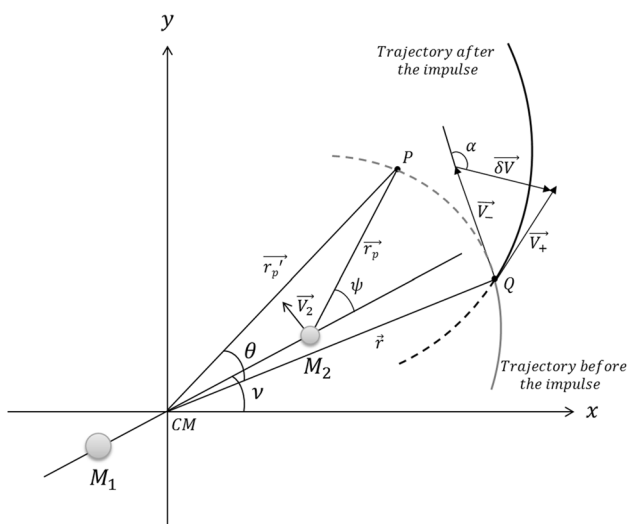


Fig. 1 PSBM in an elliptic system

imaginary continuation of this orbit (without thrust). From the point Q , the black continuous line represents the trajectory of the space vehicle after the application of the impulse. The dashed black line represents the imaginary part of this trajectory, which would exist if the trajectory was the one obtained after the application of the thrust. θ is the angle between \vec{r}_p' and \vec{r} . x_p' and y_p' are the components of the vector \vec{r}_p' , which is the periapsis position vector with origin in the center of mass of the fixed system (CM); x and y are the components of \vec{r} , the position vector of the space vehicle in the fixed coordinate system. If $\theta = 0^\circ$, the point Q coincides with point P [30].

The computation sequence to solve this problem has the following steps:

- (a) The parameters of the orbit are fixed (μ), and the periapsis position (x_p, y_p) and velocity (\dot{x}_p, \dot{y}_p) at the point P (Fig. 1) are obtained from the initial conditions $\psi, r_p, V_{\infty-}, e, v$, as shown in Eq. (3);

$$\begin{cases} x_p = \frac{(1-\mu)(1-e^2)}{1+e \cos v} \cos v + r_p \cos(\psi + v) \\ y_p = \frac{(1-\mu)(1-e^2)}{1+e \cos v} \sin v + r_p \sin(\psi + v) \\ \dot{x}_p = \frac{(1-\mu)e \sin v}{\sqrt{1-e^2}} \cos v - \frac{(1-\mu)(1+e \cos v)}{\sqrt{1-e^2}} \sin v - \sqrt{V_{\infty-}^2 + \frac{2\mu}{r_p}} \sin(\psi + v) \\ \dot{y}_p = \frac{(1-\mu)e \sin v}{\sqrt{1-e^2}} \sin v + \frac{(1-\mu)(1+e \cos v)}{\sqrt{1-e^2}} \cos v + \sqrt{V_{\infty-}^2 + \frac{2\mu}{r_p}} \cos(\psi + v). \end{cases} \tag{3}$$

- (b) From P , the numerical integration is performed until the spacecraft reaches point Q , whose location is obtained from $\theta = \pm \cos^{-1} \left(\frac{x_p' x + y_p' y}{r_p' r} \right)$, using the scalar product between the vectors \vec{r}_p' and \vec{r} . If θ is negative, the application point of the thrust occurs before the passage of the spacecraft by the periapsis or, if θ is positive, the application point of the thrust is after the passage of the spacecraft by the periapsis.
- (c) After the space vehicle reaches point Q , the trajectory is computationally calculated backward in time, using the equations of motion (Eqs. 1 and 2), until the space vehicle arrives at a distance that can be considered far from M_2 , such that the motion space vehicle-primary body can be assumed to be Keplerian, and the effects of M_2 are negligible.
- (d) Then, the velocity and energy of the space vehicle with respect to M_1 before the maneuver, without thrust, are measured.
- (e) Starting again from point Q , but using the initial conditions of the first numerical integration added to the components of the velocity variation given by the thrust, a new numerical integration is performed, using the equations of motion (Eqs. 1 and 2), but now forward in time. This numerical integration goes until a new large distance from M_2 is reached again. At this point,

the spacecraft is considered to be again in Keplerian motion around M_1 .

- (f) At this point, the velocity and energy of the space vehicle with respect to M_1 after the maneuver are measured.
- (g) After that, the variations of velocity and energy of the space vehicle with respect to M_1 are obtained, by directly subtracting the respective quantities involved after and before the maneuver.

3 Numerical simulations

Equation 4 gives the energy variation given by the maneuver, obtained from the difference between the energy of the space vehicle after and before the maneuver with respect to M_1 .

$$\Delta E = \left(\frac{(\dot{x}_f - \dot{x}_{1f})^2 + (\dot{y}_f - \dot{y}_{1f})^2}{2} - \frac{(1 - \mu)}{\sqrt{(x_f - x_{1f})^2 + (y_f - y_{1f})^2}} \right) - \left(\frac{(\dot{x}_i - \dot{x}_{1i})^2 + (\dot{y}_i - \dot{y}_{1i})^2}{2} - \frac{(1 - \mu)}{\sqrt{(x_i - x_{1i})^2 + (y_i - y_{1i})^2}} \right), \tag{4}$$

where (x_i, y_i) and (\dot{x}_i, \dot{y}_i) are the components of the position and velocity of the spacecraft before the maneuver (step (d) of the computational sequence shown in Sect. 2), (x_f, y_f) and (\dot{x}_f, \dot{y}_f) are the components of the position and velocity of the spacecraft after the maneuver (step (f) of the computational sequence shown in Sect. 2), both relative to M_1 ; $(x_{1i}, y_{1i}), (\dot{x}_{1i}, \dot{y}_{1i}), (x_{1f}, y_{1f}), (\dot{x}_{1f}, \dot{y}_{1f})$ are the components of the position and velocity of M_1 at the same times used to calculate the energies of the spacecraft; and μ is the mass parameter of M_2 .

From the variations of energy, it is possible to analyze the behavior of the space vehicle in the trajectory and the effects of the parameters involved.

The numerical simulations are made for a system with the same mass parameter of the Earth–Moon system, which is $\mu = 0.01214$. The sizes of the bodies and the relative distances are also taken from the Earth–Moon system, but the eccentricity of the orbits of the primaries are varied, since the goal of the present research is to analyze the effects of this parameter in the maneuver. This system is used to make the results more comparable with previous papers [19, 22, 23], where this same generalized system was used to study this problem, considering the ‘‘Circular Restricted Three-Body Problem.’’ Besides this comparison, the sizes of the bodies are used only to compute the collisions of the space vehicle with the primaries, which are not so frequent. It means that the main results obtained here are almost the same for any system of primaries with the same mass

parameter. For systems with different mass parameters, it is necessary a more detailed study, but the main results and conclusions obtained here are also valid. The value used for the periapsis distance is 10% larger than the radius of M_2 . This small value is used to obtain larger effects from the gravitational part of the maneuver, without larger risks of collisions. Regarding the approach angle, the value 270° is used, because it is the value that gives the highest energy gain in the pure gravity Swing-By [18]. The velocity of approach ($V_{\infty-}$) is adopted to be 1.0 c.u. This value was selected following [19], because it is compatible with large energy gains and few cases of captures and collisions. This quantity is also just a scale factor for the energy gains, so the results are not quantitatively different for other values. It means that keeping this value constant reduces the number of free variables, to simplify the understanding of the phenomenon.

It is also important to consider that the thrust changes the trajectory in all aspects, not only the velocity of the space vehicle. These modifications include a whole new geometry of the approach, including changes in the approach angle and the periapsis distance of the trajectory, as shown in the literature [18–23]. The values of ψ and r_p shown in the results are defined with respect to the pure gravity Swing-By. The actual values depend on the application of the thrust, which gives a new geometry for the passage.

The place where the thrust is applied can vary in the orbit of the space vehicle, but it is always inside the sphere of influence (SOI) [35] of the secondary body. In the present research, the Sphere of Hill [35] is used to define the sphere of influence of the body by:

$$R_{\text{HILL}} = \left(\frac{a(1 - e^2)}{1 + e \cos \nu} \right) \left(\frac{\mu}{3} \right)^{1/3}. \tag{5}$$

Next, computationally made color maps (Figs. 2, 3, 5, 6, 9, 10) show the energy variation (Eq. 4) of the space vehicle, with respect to M_1 , as a function of the angles that define the direction and the application position of the thrust. In total, 2,277,910 points were obtained for each map. To give a more complete view of the results, Tables 1, 2 and 3 show the largest energy variations (ΔE_{max}) and the related information for each simulation. They show the values of $\alpha, \theta, V_{\infty+}$, already defined, and R , the distance between the secondary body and the space vehicle at the moment of the application of the thrust.

Figure 2 measures how much the energy variations increase with the magnitude of the thrust, which can be seen from the values of the color scales for $e = 0.1, \nu = 0^\circ$ (at the initial time $t = 0$) and $\psi = 270^\circ$. Note the increase in the largest magnitude from Fig. 2a–f, from 1.94 to 8.35 c.u. (darker red region, in approximately $-45^\circ < \alpha < 45^\circ$ and $0^\circ < \theta < 2^\circ$), with a gradual increase between the

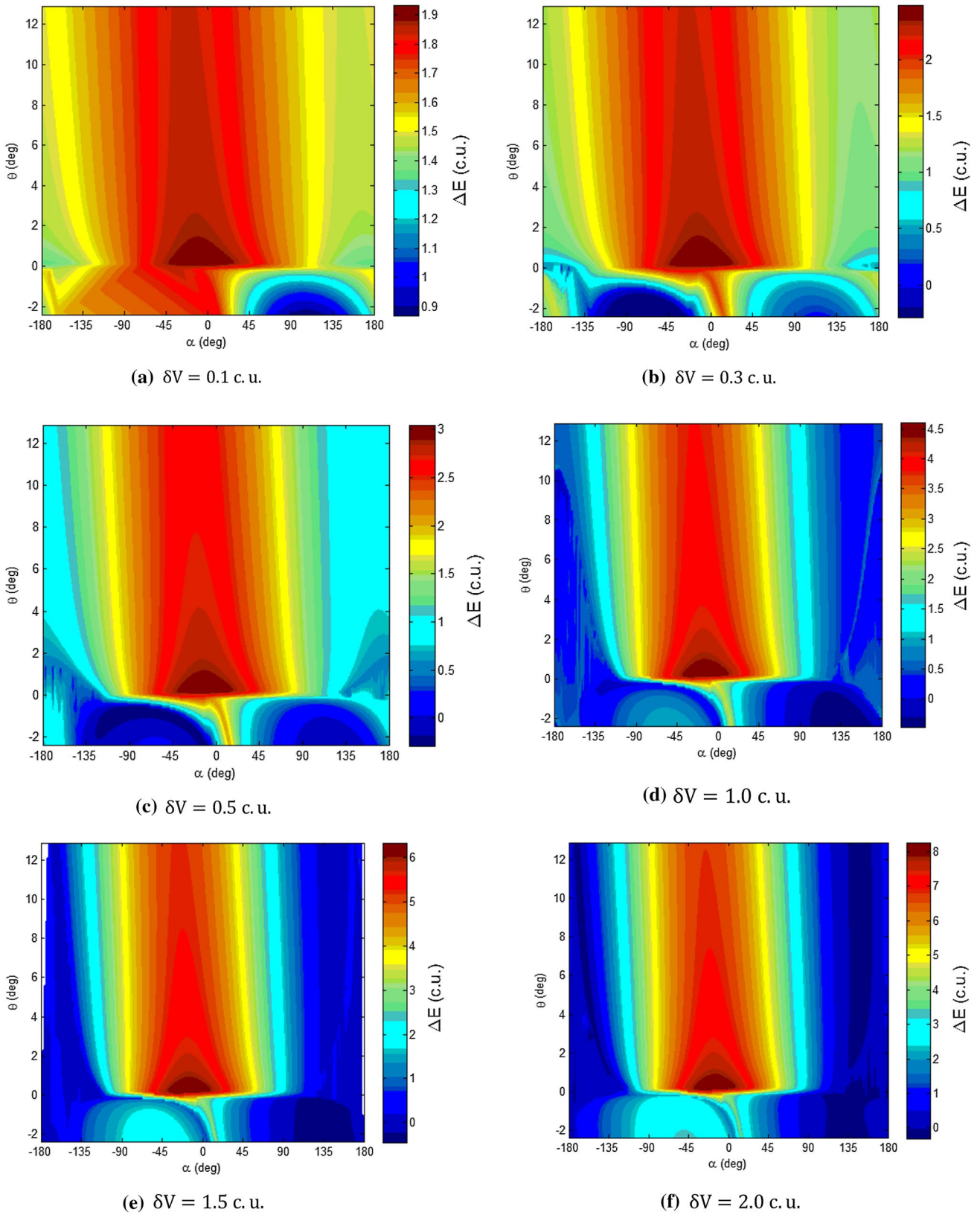


Fig. 2 Energy variations, in canonical units (c.u.), for the situation where $e = 0.1$, $v = 0^\circ (t = 0)$, $\psi = 270^\circ$ and δV in the range from 0.1 to 2.0 c.u

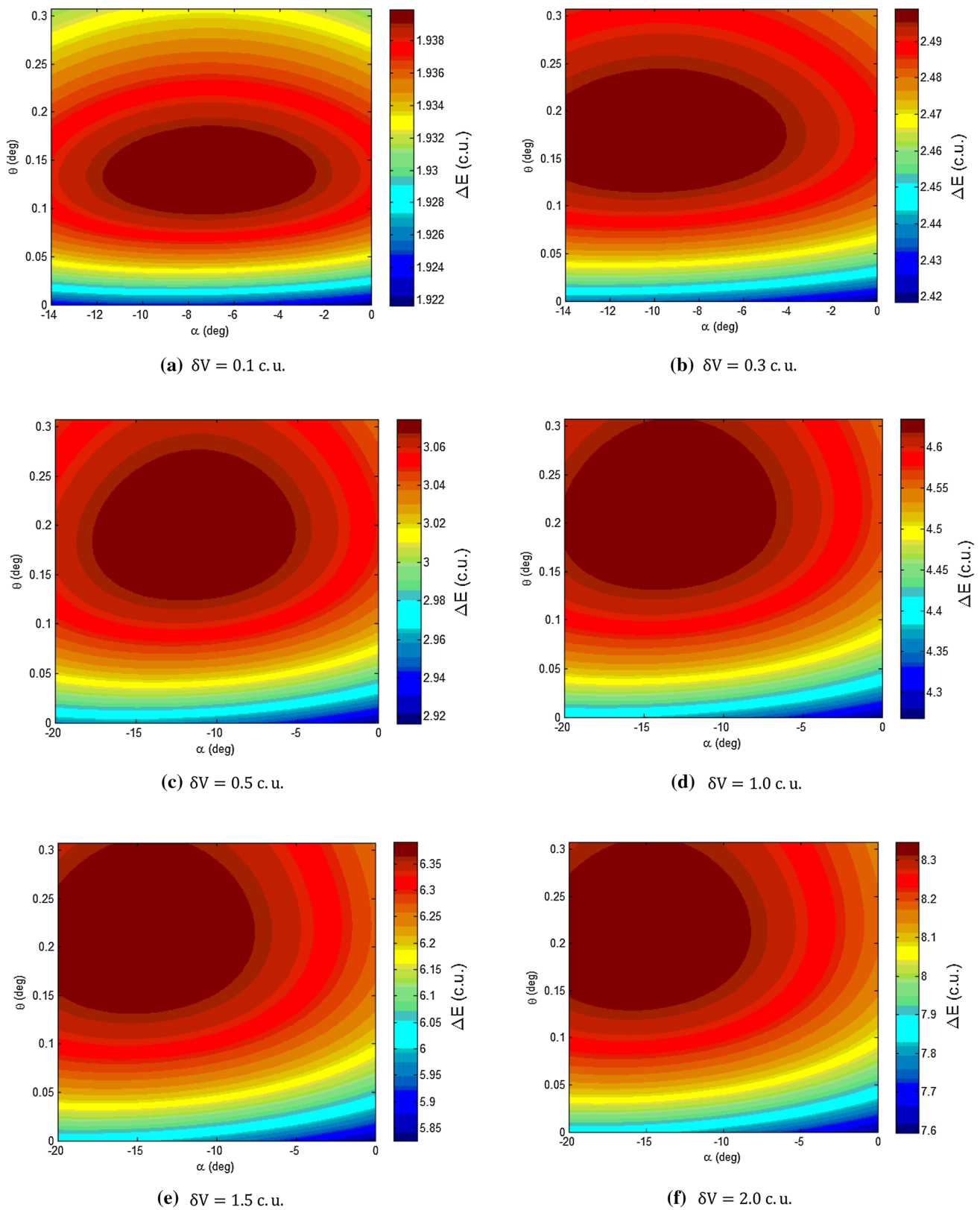


Fig. 3 Closer view of the energy variations, in canonical units (c.u.), for the situation where $e = 0.1$, $v = 0^\circ (t = 0)$, $\psi = 270^\circ$ and δV going from 0.1 to 2.0 c.u

Table 1 Information about ΔE_{\max} for $e = 0.1, \nu = 0^\circ$ and $\psi = 270^\circ$

δV (c.u.)	ΔE_{\max} (c.u.) for $\theta=0^\circ$	α (deg) for $\theta=0^\circ$	ΔE_{\max} (c.u.)	α (deg)	θ (deg)	$V_{\infty+}$ (c.u.)	R (c.u.)
0.1	1.9248	-9.0	1.9401	-7.0	0.1392	1.5577	0.0057
0.3	2.4384	-13.0	2.4996	-10.0	0.1732	1.8745	0.0060
0.5	2.9611	-16.0	3.0757	-11.0	0.1849	2.1602	0.0061
1.0	4.3881	-18.0	4.6375	-13.0	0.2086	2.7981	0.0063
1.5	6.0203	-19.0	6.3945	-14.0	0.2086	3.3922	0.0063
2.0	7.8651	-19.0	8.3535	-15.0	0.2086	3.9573	0.0063

Table 2 Information about ΔE_{\max} for $e = 0.1, \psi = 270^\circ$ and $\delta V = 0.5$ c.u

ν (deg)	ΔE_{\max} (c.u.) for $\theta=0^\circ$	α (deg) for $\theta=0^\circ$	ΔE_{\max} (c.u.)	α (deg)	θ (deg)	$V_{\infty+}$ (c.u.)	R (c.u.)
0	2.9611	-16.0	3.0757	-11.0	0.1849	2.1602	0.0061
90	3.0262	-17.0	3.1241	-14.0	0.1274	1.9148	0.0058
180	2.9385	-22.0	3.0457	-19.0	0.1145	1.8697	0.0059
270	2.8480	-21.0	2.9740	-17.0	0.1672	2.1034	0.0062

Table 3 Information about ΔE_{\max} for $\nu = 0, \psi = 270^\circ$ and $\delta V = 0.3$ c.u

e	ΔE_{\max} (c.u.) for $\theta=0^\circ$	α (deg) for $\theta=0^\circ$	ΔE_{\max} (c.u.)	α (deg)	θ (deg)	$V_{\infty+}$ (c.u.)	R (c.u.)
0	2.3618	-17.0	2.4216	-14.0	0.1352	1.7254	0.0059
0.1	2.4384	-13.0	2.4996	-10.0	0.1732	1.8745	0.0060
0.3	2.6180	-5.0	2.6793	-2.0	0.2949	2.2938	0.0062
0.5	2.9804	4.0	3.0384	6.0	0.5832	2.8622	0.0065

intermediate values of δV . Also note that, the lowest values of energy variation occur for approximately the same geometry ($\alpha > 45^\circ$ and $\theta < 0^\circ$), but the magnitude decreases, reaching negative values of ΔE in case Fig. 2f, i.e., largest loss (darker blue region). This is of course expected, since thrusts with larger magnitudes can provide more energy to the space vehicle. But, even expected, the results presented here are important to quantify these increases, which is difficult to estimate without performing the computational studies made here. The dynamics involved is very complex, due to the modification of the geometry during the maneuver, and it is necessary to consider each case in detail.

It is also noted a strong division in the plots at the line $\theta=0^\circ$. The larger variations of energy are obtained for positive values for θ , with emphasis in the locations near zero. Note the concentration of red regions (larger variations of energy) above this line, with blue regions (smaller variations of energy) dominating the locations below this line.

Physically it means that, to maximize the energy gains, the thrust needs to be applied after the passage of the space vehicle by the periapsis, such that it can get more effects from the gravitational part of the maneuver, so increasing the variations of energy in the geometry considered in Fig. 2 ($\psi = 270^\circ$). In these circumstances, the thrust applied

changes the orbit of the spacecraft and the new periapsis can make the space vehicle to pass closer to the secondary body, increasing the variation coming from gravity effects.

In general, the lines of fixed variations of energy are near vertical, with a small inclination to the left for increasing values of θ . Therefore, to get the same variation of energy, it is necessary to decrease α when θ is increased. This is an interesting observation, because the application point of the thrust may have some constraints due to the direction of the velocity vector desired for the space vehicle after the maneuver, or even to avoid a maneuver during the periapsis passage, not to disturb observations made at the closest approach. Therefore, this compromise between α and θ may help to find the best solution considering all those aspects.

Looking at the results relative to the thrust direction, it is noticeable that the regions of the largest variations of energy are usually located in the interval of α between -45° and 0° . Since our goal is to increase the energy of the space vehicle, it is necessary to increase the effects of the gravity of M_2 in the orbit of the space vehicle. To do that, the direction of the thrust needs to point to M_2 , to bring the space vehicle closer to it, so α should be negative. The exact values of α can be seen in Table 1, which shows the cases with the largest

energy variations taken from Fig. 2, for each magnitude of the thrust.

Another effect that is noticeable is the reduction of energy when the thrust is applied against the movement of the space vehicle ($\alpha > 90^\circ$ or $\alpha < -90^\circ$). Note the concentration of red regions inside the interval $-90^\circ < \alpha < 90^\circ$. For lower values of δV the effects are smaller, and red or yellow regions are everywhere in the plots. For instance, for $\delta V = 0.1$, the energy variations are between approximately 1.4 and 1.6 c.u. for $\alpha < -90^\circ$ and $\alpha > 90^\circ$, and for $\delta V = 0.3$ the energy variations are between approximately 1.0 and 1.6 c.u. for the same extreme values of α , when considering positive values of θ in both cases.

For higher values, the color blue dominates the regions of thrusts applied against the motion of the space vehicle. Even negative values are reached, when the magnitude of the thrust is 0.3 c.u. or larger, which means that the combination of the modification of the geometry of the passage and the energy coming from the thrust can decrease the energy of the space vehicle, even if the passage occurs behind M_2 . Figure 3 shows the energy variations with a closer view in the largest energy gains region.

There are some other aspects that can be observed in Table 1 and Figs. 2 and 3. For the initial conditions studied here, the best location for the application of the thrust moves away from the periapsis, while the magnitude of the largest variations increases inside the interval $0.1 < \delta V < 1.0$ c.u. It means that it is better to wait some more time after that passage of the space vehicle by the periapsis to apply the thrust. Above magnitudes of the thrust of 1.0 c.u., there is a stabilization, and the position of the application point of the thrust remains constant for the maneuvers of largest gains. These facts can be seen from the values of θ , which increase from 0.1392° to 0.2086° and then stay constant in this value. Another observation comes from the values of R , which increases from 0.0057 to 0.0063 c.u. and then stay constant in this value. It is also noticeable that increasing the magnitude of the thrust makes the absolute value of the deviation angle for the largest energy variation to increase (see values of α). It happens because when the maneuver is applied later, it needs a larger rotation angle to change the trajectory of the space vehicle to move it closer to M_2 , to get stronger effects from the gravity.

It is also observed that the search for the application point of the thrust (case $\theta \neq 0^\circ$) gives trajectories with directions for the application of the thrust that are closer to zero, in the order of 10^{-2} . It means that the search using one more parameter can find geometries that use a little bit more of the energy directly transferred to the space vehicle by the thrust.

The energy gains obtained from the combination of the impulsive maneuver and the passage by M_2 are also observed from the values of the inertial velocity of the space vehicle after the maneuver ($V_{\infty+}$). When increasing the magnitude of

the thrust by 0.2 c.u. (from 0.1 to 0.3 c.u.), the corresponding increase in the velocity of the space vehicle after the maneuver is 0.3168 c.u. (1.8745–1.5577 c.u.), which indicates an extra gain of 0.1168 c.u. with respect to the application of the impulse. This fact happens for all the increases in the magnitude of the thrust. Looking in the largest range, the increase in the magnitude of the thrust of 1.9 c.u. (from 0.1 to 2.0 c.u.) gives an increase in the velocity of the space vehicle after the maneuver of 2.3996 c.u. (3.9573–1.5577 c.u.), an extra gain of 0.4996 c.u. Those numbers emphasize the importance of the combined maneuver studied here.

Table 1 also shows all the details of the maneuvers with largest variations of energy and a comparison of the maneuvers made with $\theta = 0^\circ$ with the situation where θ is a free variable. The exact values of the pair (α, θ) and the variations of energy are shown for both cases. It is noted that the values of θ are small, in the order of 0.1 and 0.2 degrees, but they help to increase the energy variations. In fact, the small values of θ give a first wrong impression that this variable is not important, but a value of $\theta = 0.2^\circ$ combined with the initial conditions shown in Table 1, means that the thrust is applied about 1340 km from the passage by the periapsis (distance from point P to point Q , Fig. 1), which is not a small value. The small range of values is just a consequence of the choice of this variable, which is measured from the center of mass of the system, but it is identifying locations inside the sphere of influence of M_2 .

This fact is not a problem, because it is possible to use small ranges and steps to study the effects of this variable. The amount of the energy increase depends on the magnitude of the thrust, going from 0.0153 c.u. when $\delta V = 0.1$ c.u. to 0.4884 c.u. when $\delta V = 2.0$ c.u. The angle θ also influences the values of α that gives the largest energy variation. It is observed that α moves from -9.0 to -7.0 degrees when θ goes from zero to 0.1 degrees in the situation where the magnitude of the thrust is $\delta V = 0.1$ c.u. The reason is that, when $\theta = 0.1^\circ$ degrees, the thrust is applied after the passage by the periapsis and this fact reduces the gains of sending the space vehicle in the direction of M_2 , so the magnitude of α is reduced to receive more energy from the thrust. This fact also happens for other values of the magnitude of the thrust.

This example shows the importance of leaving θ as a free parameter to get some extra energy from the thrust. Table 1 shows that an extra gain of 0.0153 c.u. (1.9401–1.9248 c.u.) is obtained when the thrust has a magnitude of 0.1 c.u. This extra energy increases with the magnitude of the thrust, reaching the value of 0.4884 c.u. (8.3535–7.8651 c.u.) when the magnitude of the thrust is 2.0 c.u.

On the opposite side, the lower values for the energy variations, for magnitudes of the thrusts from 0.1 to 0.5 c.u., occur in the region of $\theta < 0^\circ$. In these cases, the thrust is applied before the passage of the space vehicle by the point P and it changes the geometry of the close approach to reduce

the gains of energy from the gravity part of the maneuver. For $\delta V = 1.0$ c.u. and $\delta V = 2.0$ c.u., there are also smaller variations of energy for different values of θ and extreme values of α . Note the blue regions at the borders of the plots, due to the retrograde thrust, as explained before. The magnitude of the velocity when the space vehicle is leaving M_2 and the distance vehicle- M_2 are also shown in Table 1. They show the influence of the variables in the escape velocity and that the thrust is applied inside the sphere of influence of M_2 , which is 0.1434 (for $e = 0.1$ and $\nu = 0^\circ$).

Another observation about θ is shown in the maps of Fig. 18, in “Appendix 2.” It shows the differences between the energy variations shown in Fig. 2 and the energy variations obtained with the same conditions used in Fig. 2 and $\theta = 0^\circ$. A positive difference means that to apply the impulse with a nonzero θ is the best option to increase the energy variation of the space vehicle. If the difference is negative, $\theta = 0^\circ$ is the best option for increasing ΔE . From Fig. 18b–f, the white region at the edges of the graph is conditions with $\theta = 0^\circ$ that results in captures or collisions of the space vehicle by the secondary body, making comparisons impossible and allowing $\theta \neq 0^\circ$ to be the best option, when it does not result in a capture or collision. For $\delta V = 0.3$ (Fig. 18b) onward, $\theta > 0^\circ$ is always better in terms of increasing energy variations, when compared with $\theta = 0^\circ$. For solutions using up to $\delta V = 0.5$, ΔE is larger than $\Delta E_{\theta=0^\circ}$ for $\alpha < -90^\circ$ and $\alpha > 90^\circ$. For $\delta V = 1.0$, the largest differences occur when θ is around 0° and 2° . Note that the magnitude of the impulse influences directly the analysis of the effects of θ .

Considering now the problem of quantifying how much the impulsive maneuver contributed to the energy gain process, we compute the energy variation given by the maneuver by applying the maneuver in a point far from M_2 (ΔE_{after}), outside its sphere of influence (after the closest approach) and in the direction of the spacecraft’s movement, to get maximum energy from the impulse. Figure 4 shows this rate for the conditions shown in Fig. 2. Since we have $\alpha = \theta = 0$, there is a single value for each δV , which, if subtracted from the magnitude available in the color maps shown in Fig. 2, give us the extra energy gain due to the thrust. For example, for $\delta V = 2.0$, $\Delta E_{\text{after}} = 7.2$ c.u., i.e., Considering that $\Delta E_{\text{max}} = 8.35$ c.u. (Fig. 2f), we know that the application of the impulse inside the sphere of influence of M_2 (and not in a distant point after the close approach) give us an extra gain of energy of approximately 1.15 c.u., for the initial conditions adopted.

Analyzing the trajectories in some more detail, we verified that there are some occurrences of captures and collisions, as presented in Sect. 3.1. Except when $\delta V = 0.1$ c.u., when the effects of the thrust is not large enough to cause captures, the captures and collisions occurred for the extreme values of α and θ . In the color maps, they appear as

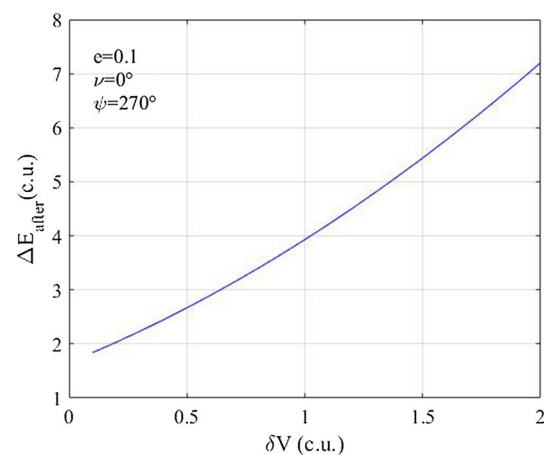


Fig. 4 Energy variation (ΔE_{after}) as function of δV , for $e = 0.1$, $\nu = 0^\circ$ and $\psi = 270^\circ$, for the pure gravity Swing-By maneuver and with the impulse applied outside the SOI of M_2

a thin white region (for example, in Fig. 2e), or they do not even appear, because they are in the borders of the maps.

The eccentricities of the orbits of the primaries also have an important role in the maneuver. The velocity of M_2 relative to the center of mass (V_2), which is constant in the circular system, is now variable and it depends on the true anomaly ν of M_2 in its orbit around of the center of mass of the system. If $\nu = 0^\circ$, M_2 is in the periapsis of its orbit around of the center of mass of the system, and V_2 is maximum. On the other side, if $\nu = 180^\circ$, M_2 is at the apoapsis of its orbit around of the center of mass of the system, and V_2 is minimum. This is a very important point, because the energy variation is dependent on V_2 , as shown in Eq. 6 (obtained from [36]), for $\theta = 0^\circ$.

$$\Delta E = \frac{1}{2} (V_{\infty+}^2 - V_{\infty-}^2 - 2V_2 V_{\infty-} \sin(\beta - \delta + \psi) + 2V_2 V_{\infty+} \sin(\beta - \delta + \Theta + \psi)), \tag{6}$$

where $V_{\infty-}$ and $V_{\infty+}$ are the approach and departure velocities of the spacecraft with respect to M_2 , respectively; β is the angle between \vec{V}_2 and the line connecting the primaries; δ is the deflection angle of the first part of the maneuver, and Θ the total deflection angle of the maneuver, which depends on the parameters of the impulse.

Based on these facts, the effects of the eccentricity and the true anomaly in the results are verified in the present research. Figure 5 shows the energy variation obtained from trajectories with $e = 0.1$, $\psi = 270^\circ$ and $\delta V = 0.5$ c.u., for true anomalies of M_2 equal to 0° , 90° , 180° and 270° . Note that the energy variation is in the same color scale for all figures, to facilitate the comparisons.

The best energy variations are obtained when $\nu = 0^\circ$ and they are larger than the same value measured when $\nu = 180^\circ$.

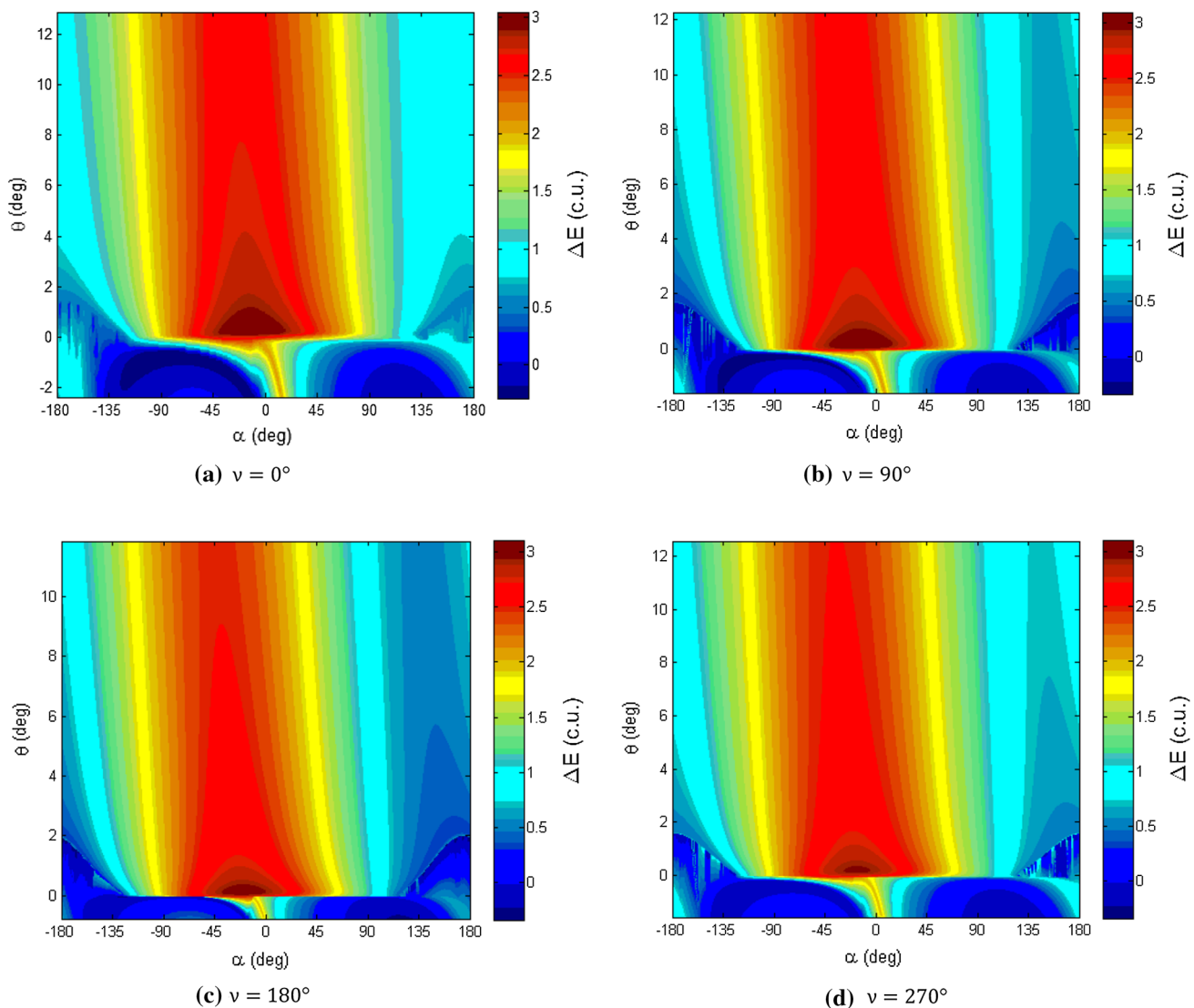


Fig. 5 Energy variations, in canonical units (c.u.), for the situation where $e = 0.1$, $\psi = 270^\circ$ and $\delta V = 0.5$ c.u

This can be seen from the darker red and light blue regions comparing the two cases. The reason is the largest velocity of the secondary body with respect to the main body. In fact, without the presence of the thrust, the expected results would be that the variations of energy would be maximum when $\nu = 0^\circ$ and minimum for $\nu = 180^\circ$. The application of the thrust changes the geometry and destroys this sequence in some cases. In the present example, the largest ΔE_{\max} occurs at $\nu = 90^\circ$ (see Fig. 7 and Table 2), but the darker red and light blue regions of the figures show that this sequence is followed in the majority of the cases.

The angle θ also plays an important role in this condition, and the magnitudes of the largest energy variations are functions of this variable. In all conditions studied here, the thrusts are applied after the passage of the space vehicle by the periapsis, allowing the space vehicle to receive as

much energy as possible from the gravity of the body. Figure 6 shows the energy variations with a closer view in the region of largest energy gains. Note that, for all values of ν , the largest variations of energy occur for negative values of α , because thus geometry sends the space vehicle to the direction of M_2 to take more advantage of the effect of its gravity, which is working in favor of energy gains in this geometry. Figure 6 also shows that θ is positive, i.e., the thrust is always applied after the passage of the space vehicle by the periapsis of its orbit and toward the secondary body. This configuration allows the space vehicle to take more advantage of the effect of the gravity of M_2 .

Table 2 shows the same details available in Table 1, but now for the situation where the true anomaly is varied according to Fig. 5. The analysis is done for $e = 0.1$, $\psi = 270^\circ$, $\delta V = 0.5$ c.u. and the particular cases

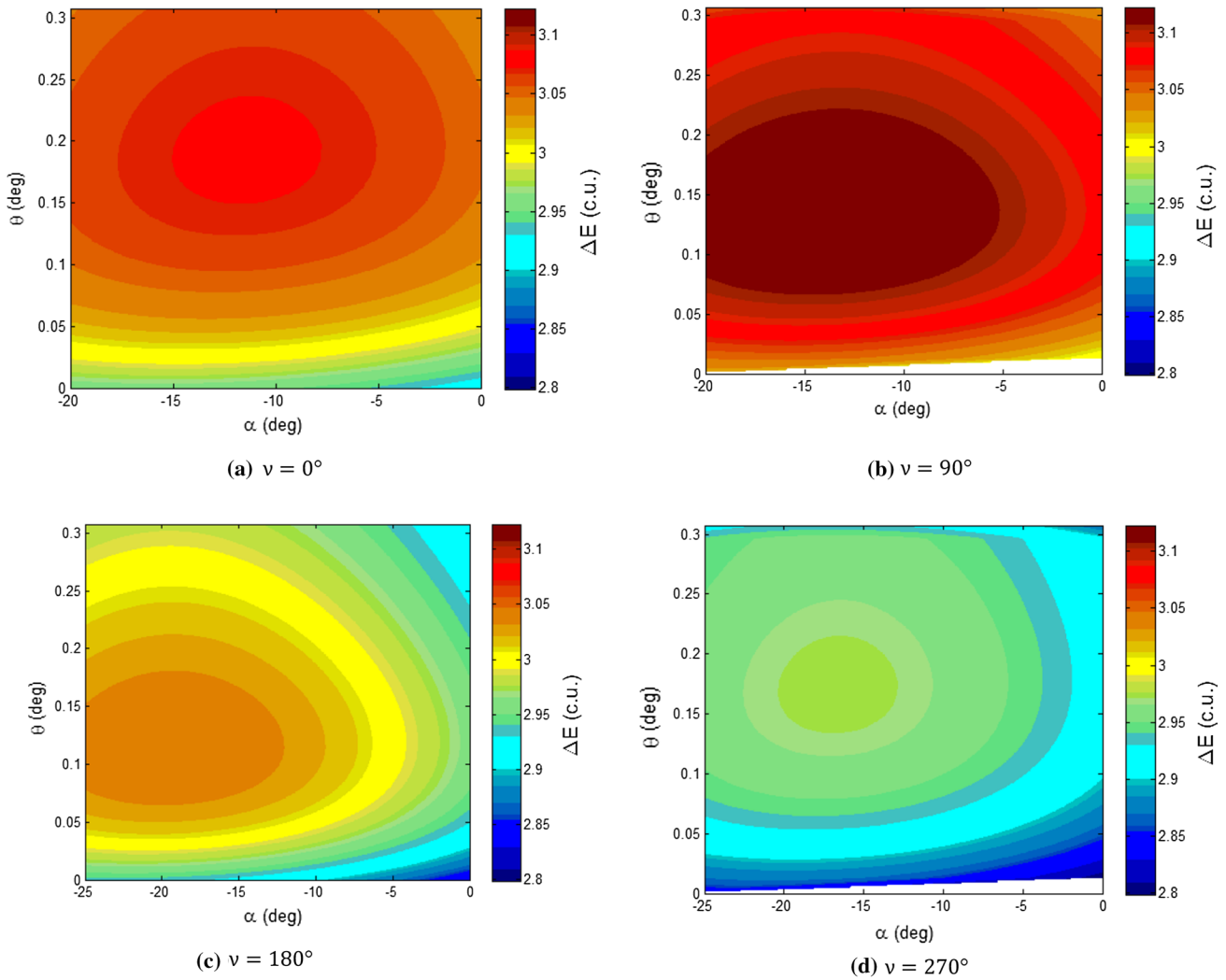


Fig. 6 Closer view of the energy variations, in canonical units (c.u.), when $e = 0.1$, $\delta V = 0.5$ c.u. and $\psi = 270^\circ$

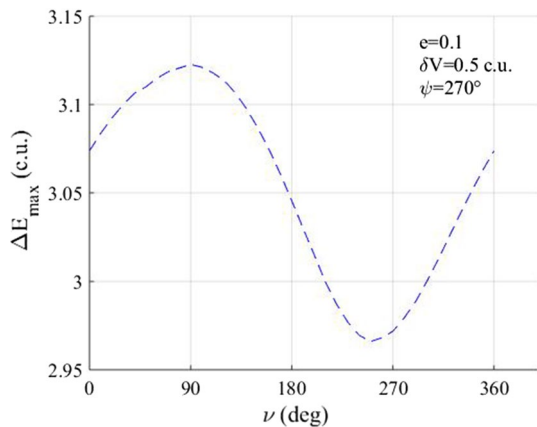


Fig. 7 Largest energy variation as function of the true anomaly (ν) for $e = 0.1$, $\delta V = 0.5$ c.u. and $\psi = 270^\circ$

$\nu = 0^\circ, 90^\circ, 180^\circ$ and 270° . The highest value of the energy variation occurs when $\nu = 90^\circ$. This behavior is due to the influence of the thrust. When considering the pure gravity maneuver, the larger variations of energy occur when the secondary body is in the periaapsis of its orbit ($\nu = 0^\circ$) [37]. We confirm these data in Fig. 7, when we test the complete range of ν , for the conditions $e = 0.1$, $\delta V = 0.5$ c.u. and $\psi = 270^\circ$. We call the largest energy variation “ ΔE_{\max} .” The escape velocity and the distance between the space vehicle and M_2 at the time of the application of the thrust are also presented in Table 2.

It is also observed from those results (Table 2, Figs. 5, 7) that the largest energy variation is dependent on the true anomaly. It is higher for $\psi = 270^\circ$, when $\nu = 90^\circ$, followed by $\nu = 0^\circ, \nu = 180^\circ$, and $\nu = 270^\circ$, respectively. The differences are of the order of 0.1 c.u., about 3.5% of the total variations. It means that extra gains of energy are obtained from the best position of M_2 at the moment of the closest

approach, if this choice does not impact in other constraints of the mission. The same sequence of true anomalies is followed when the position of the application point (θ) is fixed in zero or optimized, but the magnitudes of the variations of energy are higher when this location is optimized. They are about 0.1 c.u. higher, which corresponds to about 3.5%.

This search for the best values also decreases the angle between the thrust and the direction of motion, getting more energy from the thrust, as explained before. Those results are obtained from the numerical computation of this complex dynamics, and it is not possible to make predictions based on simple models. This is one of the main reasons to make numerical studies of this type.

The comparison between the energy variations shown in Fig. 5 and the energy variations obtained with the same conditions of Fig. 5, but with $\theta = 0^\circ$, is shown in the maps available in Fig. 19, “Appendix 2.” We see there that, for the cases analyzed, the application of the impulse in the vicinity of the periapsis ($\theta \neq 0^\circ$) is recommended when the direction of the impulse (α) tends to values smaller than -90° or greater than 90° , and with $-90^\circ < \alpha < 90^\circ$ and θ in a narrow region approximately between 0° and 1° . The difference $\Delta E - \Delta E_{\theta=0^\circ}$ reaches around 1.5 c.u.

About the extra energy gain obtained due to the application of the thrust, for the conditions shown in Fig. 5, we have the ΔE_{after} in Fig. 8, for $\nu = 0^\circ$, $\Delta E_{\text{after}} = 2.668$ c.u.; for $\nu = 90^\circ$, $\Delta E_{\text{after}} = 2.505$ c.u.; for $\nu = 180^\circ$, $\Delta E_{\text{after}} = 2.31$ c.u. and for $\nu = 270^\circ$, $\Delta E_{\text{after}} = 2.479$ c.u. These values can be applied to the magnitudes of the maps available in Fig. 5, thus calculating the extra gain.

For a more complete and comprehensive analysis, we combine different values of true anomaly (ν) and ψ . For each combination, we performed several combinations of α and θ to compute the energy variations. From this, we take

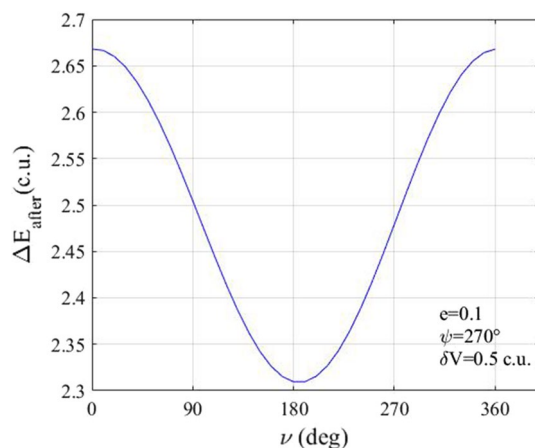


Fig. 8 Energy variations (ΔE_{after}) as function of ν , for $e = 0.1$, $\psi = 270^\circ$ and $\delta V = 0.5$ c.u., for the pure gravity Swing-By maneuver and with the impulse applied outside the SOI of M_2

the best values of α and θ for the largest energy variation and generated the three maps shown in Fig. 9, for $e = 0.1$ and $\delta V = 0.5$.

Note that ψ has a stronger influence on the energy variations compared to the true anomaly, since the curves are closer to vertical (Fig. 9a). The largest gains tend to occur for ψ approximately between 270° and 360° , with a largest value of $\Delta E_{\text{max}} = 3.27$ c.u., occurring for $\psi = 300^\circ$, $\nu = 175^\circ$, $\alpha = -11^\circ$ and $\theta = 0.11^\circ$. In the region of $270^\circ < \psi < 360^\circ$, α varies approximately between -25° and 6° , with the best values, in terms of larger energy variations, occurring for negative α (Fig. 9b). This is expected, since this region corresponds to gains of energy, therefore sending the spacecraft in the direction of the secondary body can help to increase the energy gains due to the gravity.

To summarize these results and to simplify the analysis, we show ΔE_{max} and their respective direction (α) and point of application (θ) of the thrust as a function of ψ , for ν equal to 0° , 90° , 180° and 270° , $\delta V = 0.1, 0.3, 0.5, 1.0$ c.u. and eccentricity equals to 0.1 (Fig. 10).

Several observations can be made from those results. The first one is that Fig. 7 consolidates these results for $\delta V = 0.5$ c.u. Another observation is that the largest energy variations follow approximately the behavior expected for the unpowered Swing-Bys for lower values of the thrust (see in particular the situation where the thrust is 0.1 c.u.). For $\delta V = 0.1$ c.u., there is a large gain of energy around $\psi = 270^\circ$, a large loss around $\psi = 90^\circ$ and near zero variations for $\psi = 0^\circ$ and 180° [18], for the values of ν analyzed in Figs. 5 and 6. Larger values for the thrust change the dynamics, and the higher values for the variations of energy are then located near $\psi = 315^\circ$ with the lower variations occurring for $\psi = 180^\circ$ (see in particular the situations where the thrust is 1.0 c.u.). For instance, in Fig. 10a, for $\delta V = 1.0$ c.u., the pink curve on the ΔE_{max} plot shows $\Delta E_{\text{max}} = 5.07$ c.u. for $\psi = 315^\circ$ and $\Delta E_{\text{max}} = 1.85$ c.u. for $\psi = 180^\circ$, as the extreme values of the curve. This is a new and important result, which can be obtained only by the computational simulations presented here and has a direct impact in mission planning.

Regarding the effects of the magnitude of the thrust in the variations of energy, for all values of the true anomaly, the largest variations in energy are always obtained using the largest thrust of 1.0 c.u. In those large values, all the variations of energy are positive, even for geometries where the gravity part of the maneuver removes energy from the space vehicle (ψ in the range $0^\circ - 180^\circ$). But, for lower values of the magnitude of the thrust, which are more practical from the engineering point of view, there are overlaps in the lines of variations of energy. It means that there is an important effect coming from the approach angle and, depending on the value of this angle, it is possible to get larger variations of energy from lower values of the thrust. It happens because

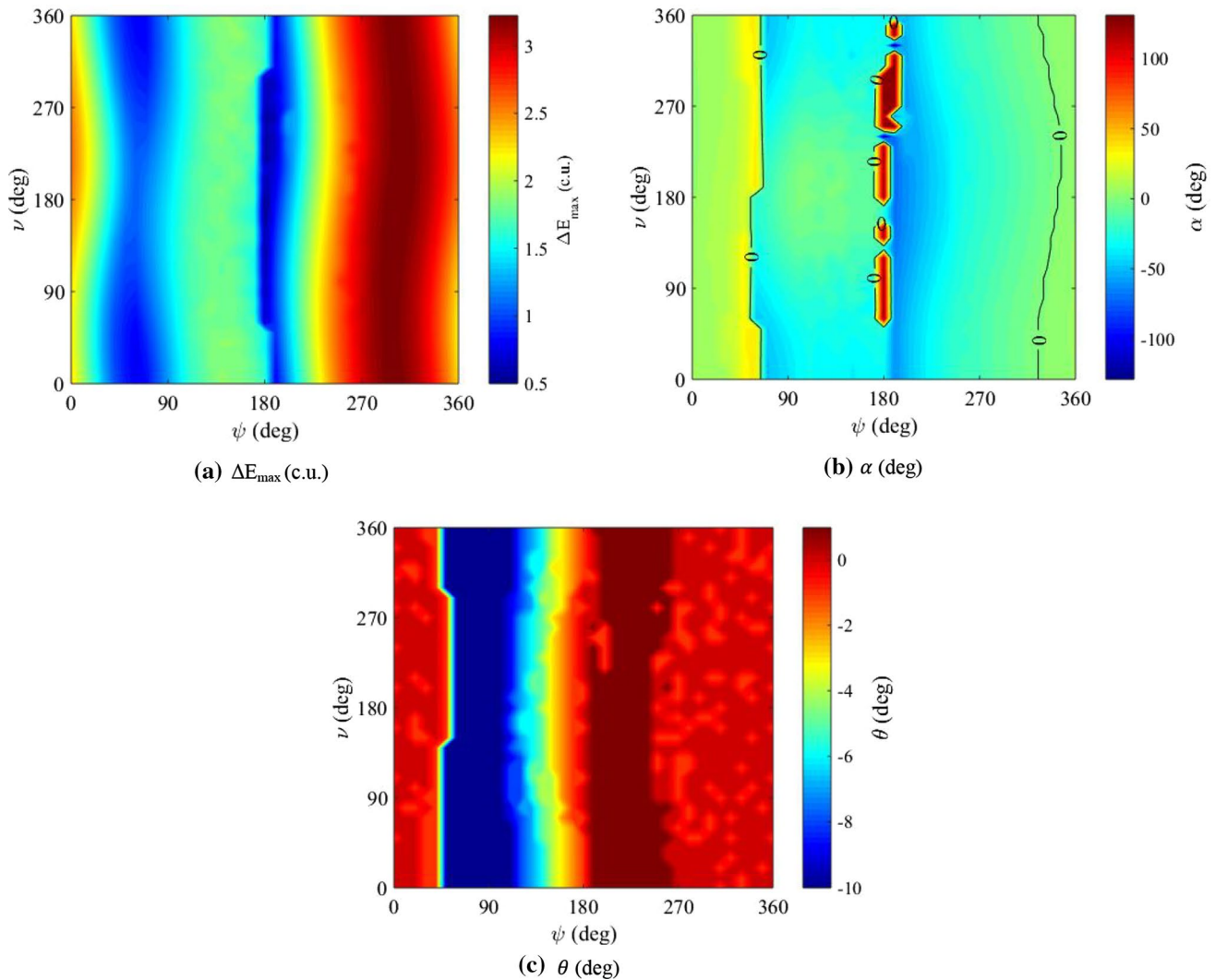


Fig. 9 **a** Largest energy variations, ΔE_{\max} (in canonical units), **b** respective values of α for ΔE_{\max} (in degrees) and **c** respective values of θ for ΔE_{\max} (in degrees), when $e = 0.1$ and $\delta V = 0.5$

the geometry made a better use of the combination of impulsive maneuver and close approach.

Analyzing the results with respect to the direction and location of the thrust, different behaviors are noted depending if the approach angle is smaller or larger than 180° . This happens because the goal of the maneuvers studied here is to maximize the energy gains, and the geometry to receive more energy from the gravitational part of the maneuver occurs for angles of approach larger than 180° . This is the best range to get increases in energy. The complete range $0 - 360^\circ$ is studied here because other constraints of the mission may limit those values, so it is interesting to know the complete results.

For $\psi = 180^\circ$, the deviation angle is always negative, in the range 0° to -20° , to send the space vehicle to the direction of the secondary body to increase the gains from the gravity part of the maneuver. For angles of approach smaller

than 180° , there are oscillations of positive and negative values, depending on the geometry of the approach and the magnitude of the thrust. The maneuver tries to minimize the loss of energy from the gravity of the Swing-By. There is also the effect of the larger magnitudes of the thrust, that dominates the scenario and changes the results expected based on the pure gravity maneuver.

Looking at the results for the location of the thrust, it is noted that, for angles of approach larger than 180° , there are usually smaller positive values. It means that the impulsive maneuver is made after the passage by the periapsis, to get stronger effects from the gravitational part of the maneuver. This is done because the maneuver is giving energy to the space vehicle. For angles of approach smaller than 180° , there are usually larger negative values. It means that the impulsive maneuver is applied before the passage of the space vehicle by the periapsis, to change the geometry of

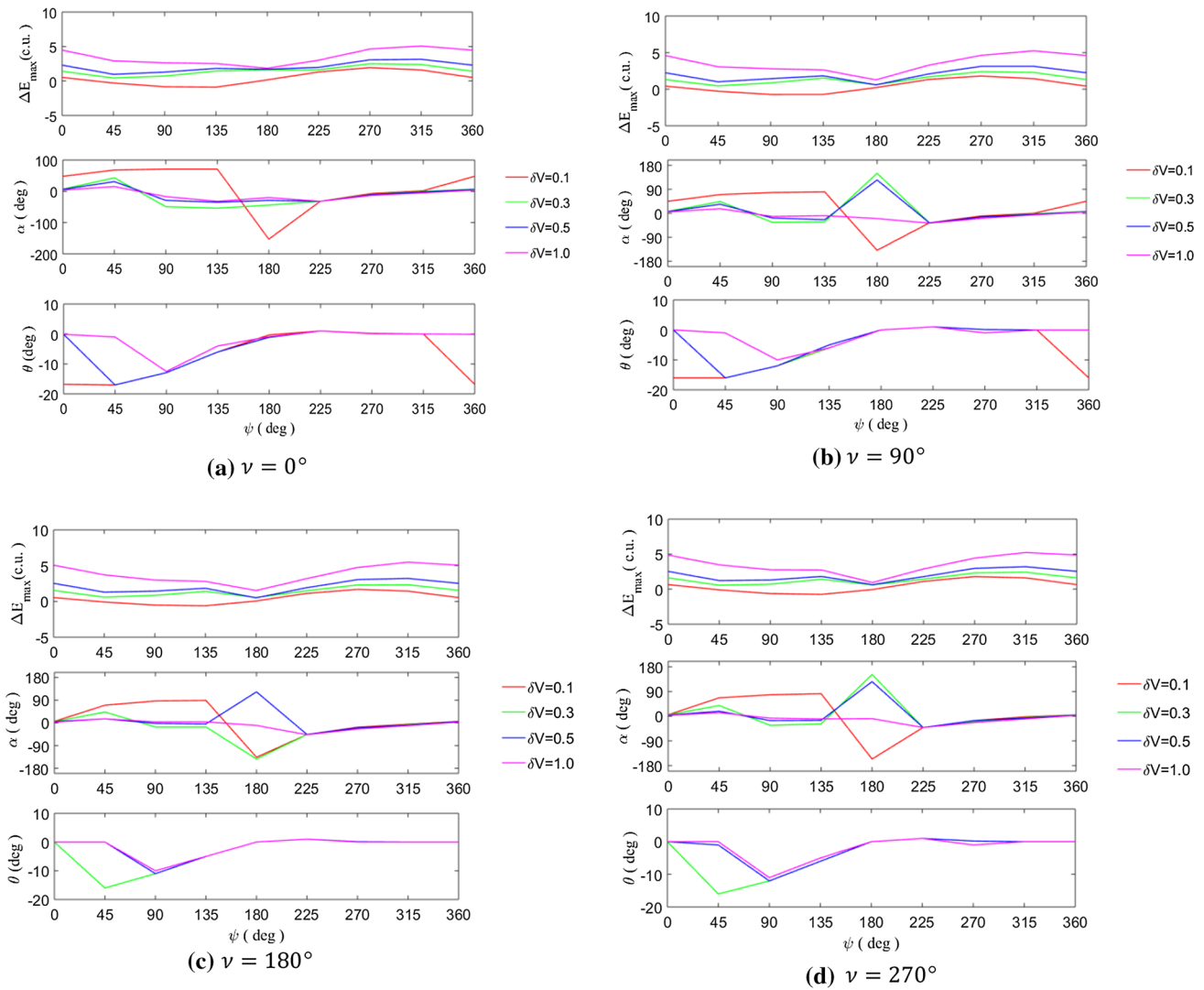


Fig. 10 Largest energy variations, directions and thrust locations for $e = 0.1$

approach to reduce the removal of energy coming from the gravity effects. Exceptions are found for very large impulsive maneuvers, where the thrust dominates the scenario. Those behaviors are similar for all the true anomalies studied here, just with some differences in the magnitudes.

Next, we derived empirical equations based on the computational simulations made here to describe the curves shown in Fig. 10. These equations were obtained from the fitting function of the numerical program and can be used to make a fast calculation of the energy variations and to show the general behavior of the variables as a function of the parameters of the maneuver. The equation given by a 6-order polynomial is close enough to the curve, regardless of the number of points evaluated. In this case, it can be applied to a system with mass parameter similar to the one of the Earth–Moon system ($\mu = 0.01214$), $V_{\infty-} = 1.0$ c.u. and $e = 0.1$. After fixing these values, the equations are

written as a function of the variables related to the approach angle (ψ), true anomaly (ν) and magnitude of the thrust applied (δV). When $n = 1$, we have the equation related to Fig. 10a, for $\nu = 0^\circ$. For $n = 2$, the equation represents the results shown in Fig. 10b, for $\nu = 90^\circ$. For $n = 3$, the equation is valid for Fig. 10c, when $\nu = 180^\circ$ and $n = 4$ considers the case shown in Fig. 10d, with $\nu = 270^\circ$. Note that all the coefficients are functions of the magnitude of the thrust (Eq. 9, “Appendix 1”), so this variable is still present in the equations.

$$\Delta E_{\max} = a_n \psi^6 + b_n \psi^5 + c_n \psi^4 + d_n \psi^3 + e_n \psi^2 + f_n \psi + g_n. \tag{7}$$

The coefficients of the empirical equations for each case are shown in Eq. 9 and Table 4 of “Appendix 1.” The range of applications of the equations is limited to $\mu = 0.01214$, $V_{\infty-} = 1.0$ c.u. and $e = 0.1$, but the idea is to show an

example of the possibility of obtaining equations of this type. In terms of practical applications, the mass parameter and the eccentricity of the primaries are known for a given mission and adequate equations can be obtained in a similar form. From the preliminary mission analysis, the value of the velocity of approach is also obtained. Equation 7 is valid for any situation. It is just necessary to obtain the corrected coefficients for the equation, which can be done easily after having those three parameters. It means that it is easy to get results of this type for missions to other systems, like the planets Mars and Mercury.

The complete map of solutions of ΔE_{\max} , like for $e = 0.1$ in Fig. 9, was also made for $e = 0.05$ and $e = 0.2$ (Figs. 11, 12), since the true anomaly has a strong component that depends on the eccentricity of the system.

The first observation occurs in the energy variation (Figs. 11a, 12a). Note that, for $e = 0.05$, the curve tends to be close to vertical, with smooth waves, and, for $e = 0.2$, these waves are more prominent, showing a more significant effect of the true anomaly. This is expected, since larger eccentricities tend to increase the effects of the location of the spacecraft in its orbit. Figure 9a shows an intermediate behavior with respect to Figs. 11a and 12a. The dark red region, where the largest variations of energy occur, remains approximately between $270^\circ < \psi < 360^\circ$ in both cases. For $e = 0.05$, the largest ΔE_{\max} is 3.26 c.u., occurring for $\psi = 300^\circ$, $\nu = 182^\circ$, $\alpha = -10^\circ$ and $\theta = 0.102^\circ$. For $e = 0.2$, the largest ΔE_{\max} is 3.28 c.u., for $\psi = 304^\circ$, $\nu = 183^\circ$, $\alpha = -14^\circ$ and $\theta = 0.101^\circ$. It is also observed, in Fig. 11b, i.e., for $e = 0.05$, that α is positive for ψ around

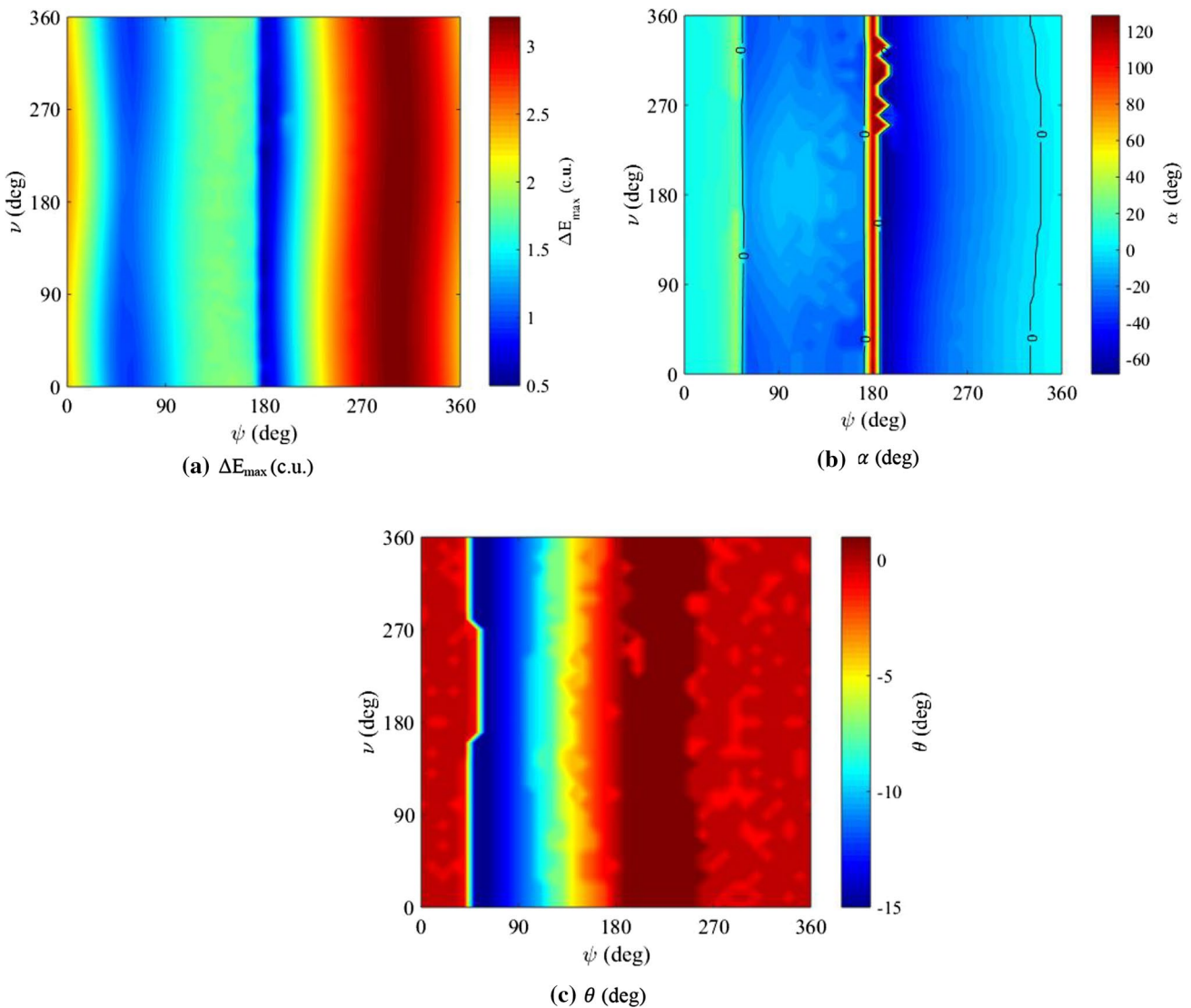


Fig. 11 a Largest energy variations, ΔE_{\max} (in canonical units), b respective values of α for ΔE_{\max} (in degrees) and c respective values of θ for ΔE_{\max} (in degrees) when $e = 0.05$ and $\delta V = 0.5$

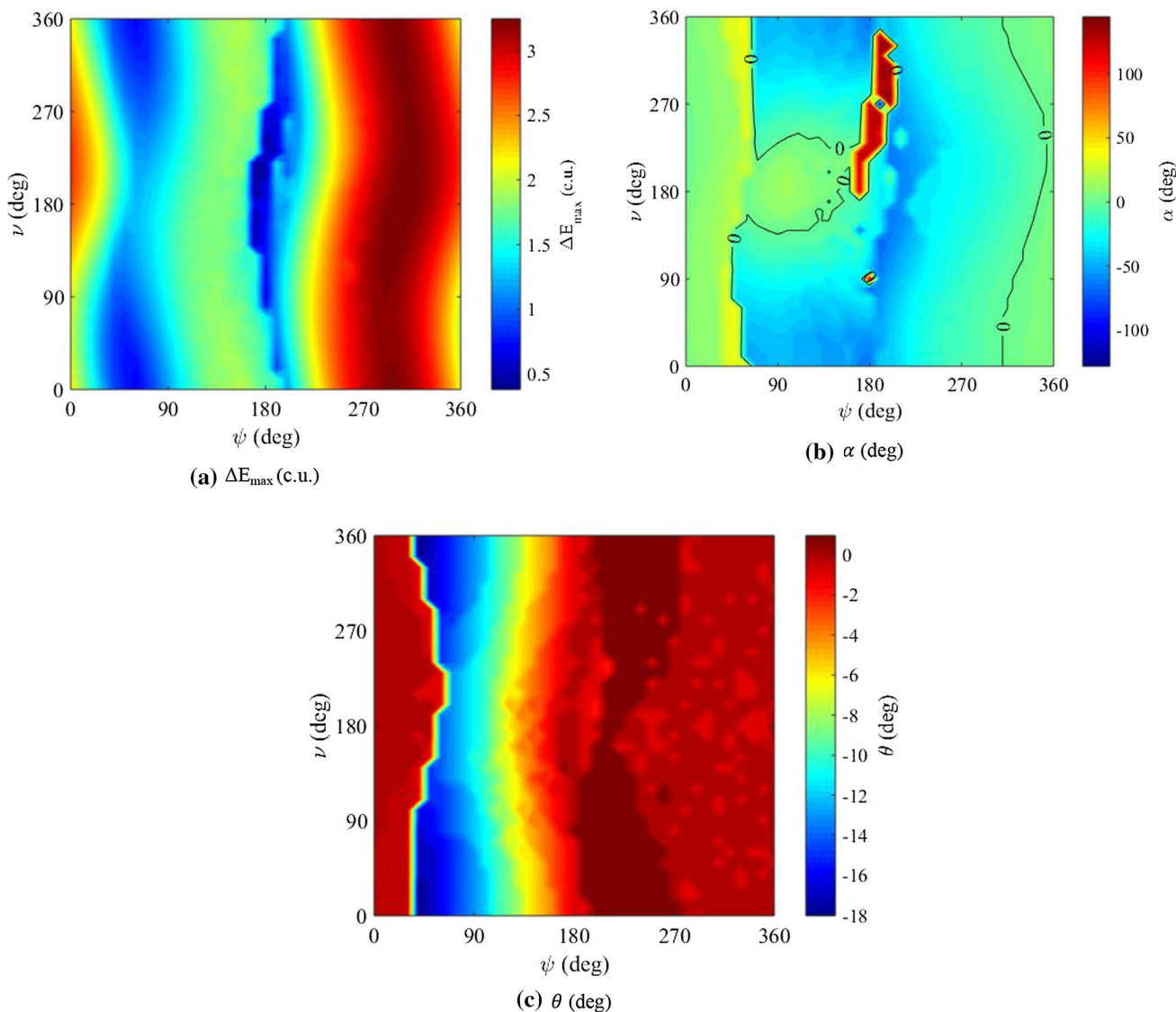


Fig. 12 **a** Largest energy variations, ΔE_{\max} (in canonical units), **b** respective values of α for ΔE_{\max} (in degrees) and **c** respective values of θ for ΔE_{\max} (in degrees) when $e = 0.2$ and $\delta V = 0.5$

180° and all values used for ν , and α is also positive for the region of $\psi < 55^\circ$ and $\psi > 335^\circ$. As the eccentricity increases, these limits become irregular but, in general, a large region around $\psi \sim 50^\circ$ to $\psi \sim 335^\circ$ has negative values for α , with a majority of values approximately between -50° and 0° . Those results are in accordance with reference [19] that showed, for a circular case, that the best direction of the impulse is around $\alpha \sim -20^\circ$.

The energy variations obtained using different eccentricities for the primaries, $\psi = 270^\circ$, $\delta V = 0.3$, as function α and θ are also studied (Fig. 13). For all the cases, M_2 is at the periapsis around M_1 during the closest approach.

Figure 14 shows the energy variations with a closer view of the largest energy gains region.

From the general characteristics of elliptical orbits, it is known that the increase in the eccentricity reduces the distance between the primaries when the secondary body is at the periapsis and that it increases this distance when the space vehicle is at the apoapsis.

Note that the regions with the highest values for the energy variations are larger for $e = 0.5$. In this case, the primaries are closer and V_2 is larger, which works in favor of the energy gains. These gains are not small, reaching values of 0.0780 c.u. (3.22%) when the eccentricity is in the range 0.0 to 0.1; and 0.6168 c.u. (25.4%), when the eccentricity goes from 0.0 to 0.5. This is of course expected, but the quantifications of those results are not easy to estimate without the

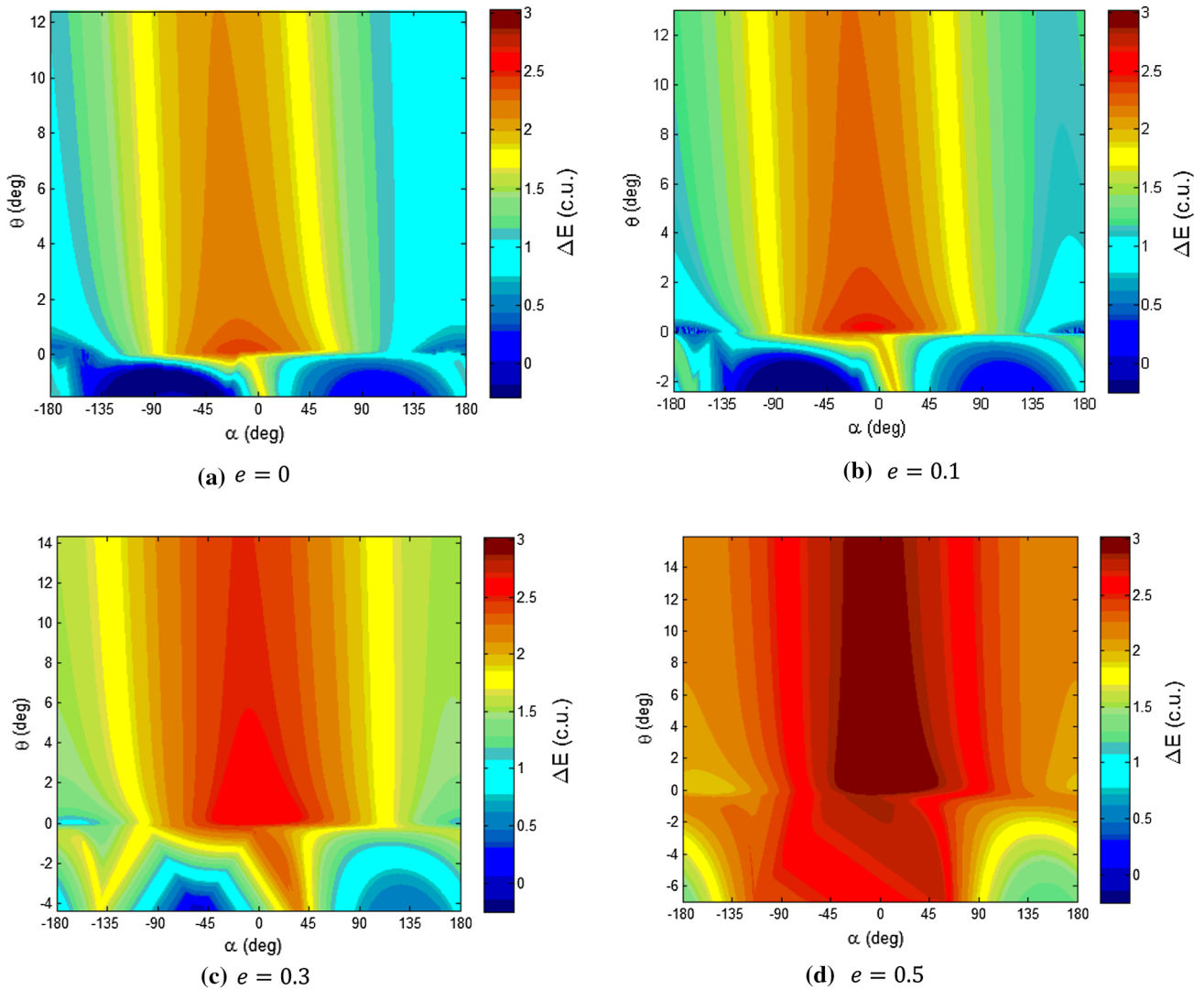


Fig. 13 Energy variations, in canonical units (c.u.), for $\nu = 0^\circ (t = 0)$, $\psi = 270^\circ$ and $\delta V = 0.3$ c.u

computational simulations made here. The ΔE_{\max} and their respective data are shown in Table 3.

From a general observation of the results, it is clear that the energy variations are proportional to the magnitude of the thrust. It is also visible that applying the thrust at a point different from the periapsis of the orbit increases the energy gains.

Figure 15 shows the energy variations for the maneuver made with the impulse applied outside the sphere of influence of M_2 (ΔE_{after}). The differences between the values of ΔE shown in the color maps of Figs. 13 and 14 and the values of ΔE_{after} , for the same initial conditions, gives the extra energy given by the thrust.

For most of the conditions, there are trajectories resulting in captures or collisions. The combination of choices for the thrust magnitude, direction and point of application of the thrust can generate optimum results, which are not

predictable from the analytical model [18, 36, 37], due to the complexity of the dynamics involved.

Some other aspects can be observed in Table 3 and Figs. 13 and 14. The location of the application of the thrust moves away from the periapsis with the increase in the eccentricity, from $\theta = 0.1352^\circ$ to $\theta = 0.5832^\circ$, when the eccentricity goes from 0.0 to 0.5, a large modification. It means that it is better to wait to apply the thrust to get more effects from the Swing-By when the eccentricity is 0.5. This effect increases with the eccentricity, since the velocity of M_2 around the main body is larger. It is also noticeable that, when $\theta \neq 0^\circ$, the directions of the application of the thrust (α) are closer to zero by a few degrees compared to the case where $\theta = 0^\circ$, with the exception of the extreme case $e = 0.5$. It happens because the search for the best solutions using one more parameter can find geometries that use a little bit more of the energy directly transferred to the space

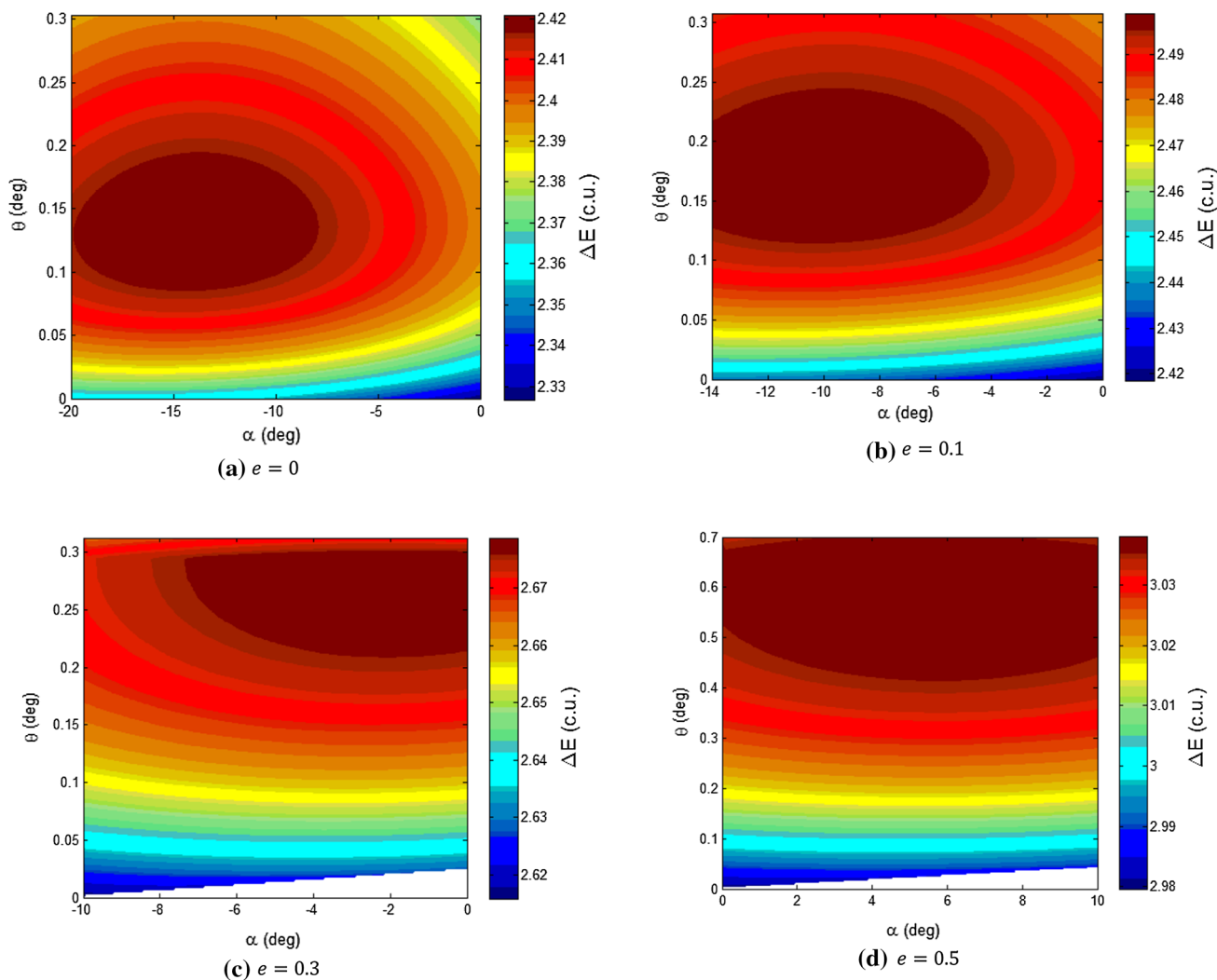


Fig. 14 Closer view of the energy variations, in canonical units (c.u.), for $\nu = 0^\circ (t = 0)$, $\psi = 270^\circ$ and $\delta V = 0.3$ c.u. Note the different scales for the energy variation

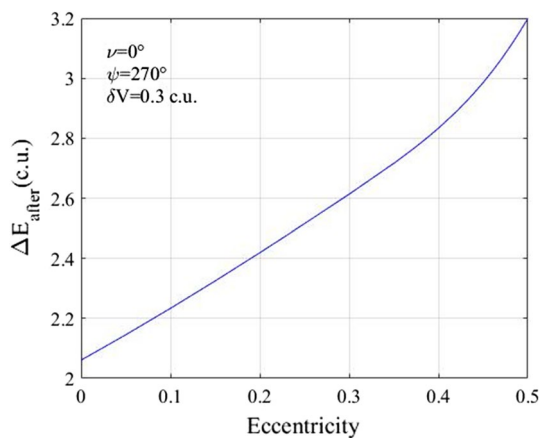


Fig. 15 Energy variation (ΔE_{after}) as function of e , for $\nu = 0^\circ$, $\psi = 270^\circ$ and $\delta V = 0.3$ c.u., for the a pure Swing-By maneuver followed by an impulse applied outside the SOI of M_2

vehicle by the thrust. The complete map of the comparison of Fig. 13 with $\Delta E_{\theta=0^\circ}$ is shown in Fig. 20, “Appendix 2.”

It is also noticeable that the larger eccentricities decrease the value of the angle that defines the direction of the impulse (α). It happens because the impulse is applied later, as just mentioned, so it tries to get more energy from the thrust. It already most of the possible energy from the gravity part of the maneuver, since it has passed by the periapsis.

The extra energy gains obtained from larger eccentricities are also observed from the values of the inertial velocity of the space vehicle after the maneuver ($V_{\infty+}$) for a given magnitude of the thrust. When increasing the eccentricity from 0.0 to 0.1, there is an increase in the velocity of the space vehicle after the maneuver of 0.1491 c.u. (1.8745–1.5577 c.u.). This extra velocity goes up to 1.1368 c.u., when the eccentricity is 0.5. These increases show the importance of

considering the eccentricity of the primaries in the maneuvers studied here.

Next, the effect of the eccentricity in ΔE_{\max} is shown in Fig. 16. The direction and thrust location are also shown. The analysis was performed for eccentricities varying from 0.01 to 0.7, $\nu = 0^\circ$ and $\psi = 270^\circ$ (because it is the region of largest energy gain due to gravity) and different values of the thrust. The results confirm the observations made based on Table 3, but now for a large range of eccentricities.

The empirical equation for ΔE_{\max} is valid for a system with mass parameter similar to the Earth–Moon ($\mu = 0.01214$), $V_{\infty-} = 1.0$ c.u., $\nu = 0^\circ$ and $\psi = 270^\circ$ and variable eccentricity and magnitude of thrust are shown in Eq. 8. The coefficients are available in Table 4, in “Appendix 1.” The same comments made for Eq. 7 apply here. The idea is to show an example of an equation of this type. It is valid for any system of primaries, if the coefficients are correctly obtained for a specific situation, like missions to Mars or Mercury.

$$\Delta E_{\max} = a_5 e^2 + b_5 e + c_5. \tag{8}$$

3.1 Captures and collisions

There are situations where, during the maneuver, the space vehicle is captured or it collides with the secondary body [38]. It usually occurs for extreme values of α , when the space vehicle is decelerated and sent toward M_2 . It is considered “capture” when the space vehicle remains around the body until the final integration time, i.e., approximately 3.57 years, since we adopted in the present research an integration time limit of five times the canonical unit of time,

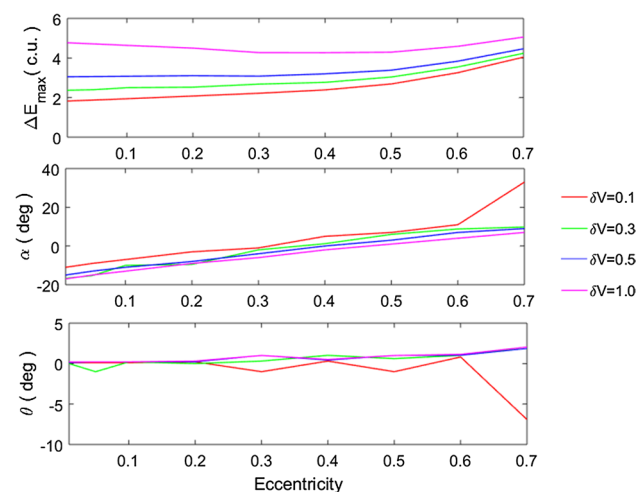


Fig. 16 Largest energy variations and the respective direction and thrust location for $\psi = 270^\circ$, $\nu = 0^\circ$ and different values for the eccentricity

and 1 c.u. time ~ 260.89 days. The analysis was done for $\nu = 0^\circ$, $\psi = 270^\circ$ and different magnitudes for the thrust. Note that the amount of captures, in general, decreases with the eccentricity. It happens because more eccentric systems have smaller periapsis distance for the primaries and larger periapsis velocity of M_2 , which consequently increases the perturbations of M_1 in the orbit of the space vehicle around M_2 , making more difficult to keep it captured around M_2 .

The numerical results also show that there is an increase in the number of captures with the magnitude of the thrust, because larger thrusts combined with geometries that favors the deceleration of the spacecraft can provide more energy to the space vehicle to reduce its velocity to be captured by M_2 . As an example, for $\delta V = 0.1$ c.u., there are no captures, while for $\delta V = 1.0$ c.u. the number of captures can go up to 1800, depending on the eccentricity of the primaries. This value is equivalent to approximately 0.08% of the total of 2,277,910 simulations for this case.

We consider a “collision” when the space vehicle hit the surface of M_2 . The analysis was made comparing the distances between the space vehicle and M_2 with the radius of M_2 . The study was done for the same conditions used in Fig. 16. It is clear that collisions are more frequent when compared to captures. It is also noticeable that the number of collisions increases with the eccentricity, in general reaching values just over 16,000 for a thrust equal to 1.0 c.u., equivalent to 0.7% of the total of simulations. It happens because the larger perturbations present in eccentric systems due to the shortest distance between the bodies and the highest velocity of M_2 contributes to make the space vehicle to collide with M_2 . Note, in Fig. 17b, that collisions occurred in all cases of eccentricities and thrusts studied, opposite to captures, which are not present in some situations.

The number of captures shown in Fig. 17a decreases with the eccentricity, but there is a peak value in $\delta V = 1.0$ and $e = 0.4$ and, after this value, the number of captures decreases. The number of collisions increases in the same region for the same configurations of α and θ and then we see that some of the captures are transformed in collisions. This fact explains the reduction in the number of captures with the eccentricity after the peak.

4 Conclusions

A numerical study of the PSBM in an elliptical system was realized to get results that are not limited by the values of the variables involved, like the eccentricity of the primaries and the magnitude of the thrust used in the maneuver.

The results show the best direction and thrust location in a PSBM. If it is considered a pure gravity maneuver, the largest variations of energy occur when the secondary body is at the periapsis of its orbit around the larger primary, due

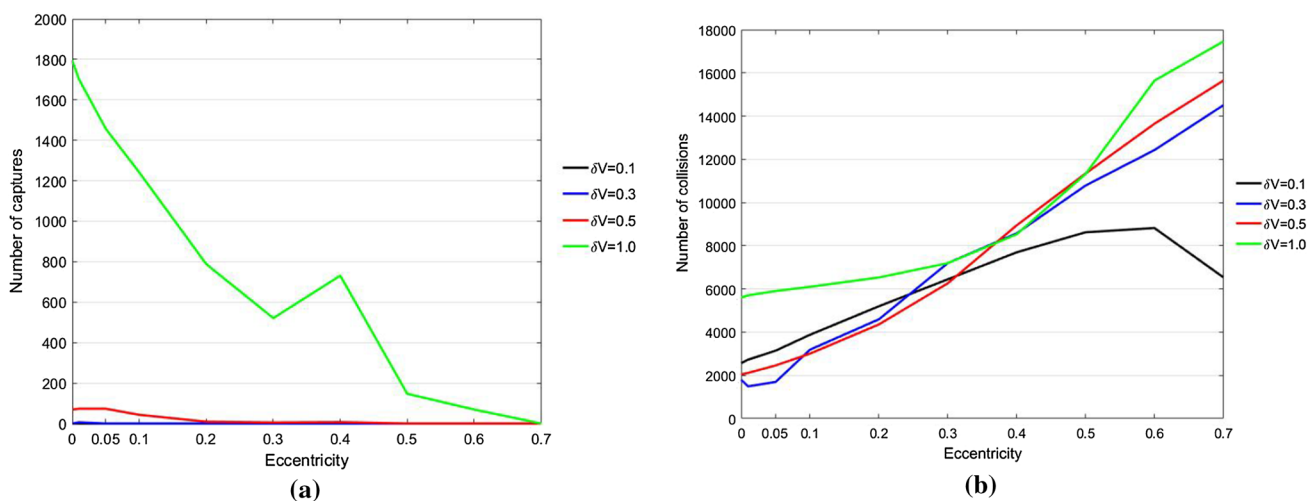


Fig. 17 a Captures and b collisions, for $\nu = 0^\circ$, $\psi = 270^\circ$ and different magnitudes of the thrust

to the strong effect of the gravity of the secondary body. However, if we apply the thrust in a non-tangential direction and not in the periapsis of the orbit of the space vehicle, the maneuver can generate larger variations of energy. The reason is the combination of the effects of the impulsive maneuver, which gives energy directly to the space vehicle, with the indirect effects of changing the geometry of the close approach. The magnitude of the thrust is varied as a free parameter, to understand better the implications of this variable.

The impulsive maneuver modifies the orbit immediately, resulting in new values for the approach angle and periapsis distance, so resulting in different geometries that can increase the energy gains. It was also noted that the position of the application point of the thrust moves away from the periapsis as its magnitude increases, in the interval going from 0.1 to 1.0 c.u., with stabilization after that point.

Empirical equations were obtained based on the numerical results obtained here for some particular cases, which can give a fast calculation of the energy variations as a function of the parameters of the maneuver. Equations similar to the ones developed here can be found for any system of primaries and approach velocity, just by adjusting the parameters of the equations.

The eccentricity of the primaries has direct effects in the results, considering the variations of the velocity of M_2 around M_1 , which is no longer constant. Our simulations varied this eccentricity in a large range, to see the effects of this important parameter. The variations of energy are directly dependent on this velocity. The results also showed that there are several situations that results in captures or escapes of the space vehicle. The number of captures decreases with the eccentricity, while the number of collisions increases, because eccentric systems are more perturbed.

In this way, this study identified the best geometry of the thrust to be applied to the space vehicle as a function of the initial parameters that describe its trajectory. This study was done for a system with parameters similar to the Earth–Moon and different initial conditions, for the purpose of studying the effects of these parameters. However, it is known that this is a maneuver that can be applied to actual systems, since the pure gravity maneuver version has already been used in missions with positive results.

The use of this powered maneuver is an important option when the energy obtained from the pure gravity Swing-By is not large enough to satisfy the mission requirements. For potential applications, there are several systems with large eccentricities in the Solar System that can be used for actual applications. As examples, Mars has an eccentricity of 0.093 around the Sun, while Mercury has an eccentricity of 0.2056. Both systems are far from circular and have been considered many times for pure gravity Swing-By maneuvers. They can also be used for powered maneuvers, like the ones shown here, with small adaptations.

Appendix 1: Coefficients of the empirical equations of ΔE_{max}

$$\text{Coef}_n = z_{10}\delta V^9 + z_9\delta V^8 + z_8\delta V^7 + z_7\delta V^6 + z_6\delta V^5 + z_5\delta V^4 + z_4\delta V^3 + z_3\delta V^2 + z_2\delta V + z_1. \tag{9}$$

See Table 4.

Table 4 Coefficients of Eq. 2, for $n = 1, 2, 3, 4$ and coefficients of Eq. 3, for $n = 5$

z_m Coef _{n}	z_{10}	z_9	z_8	z_7	z_6	z_5	z_4	z_3	z_2	z_1
a_1	-	-	-6.13e-15	9.29e-14	-5.63e-13	1.74e-12	-2.85e-12	2.3e-12	-4.52e-13	5.85e-14
b_1	-	-	4.64e-12	-7.08e-11	4.3e-10	-1.32e-9	2.09e-9	-1.52e-9	2.21e-11	-8.26e-12
c_1	-	-	-7.89e-10	1.25e-8	-7.68e-8	2.27e-7	-3.04e-7	7.97e-8	2.44e-7	-2.69e-8
d_1	-	-	-1.22e-7	1.68e-6	-9.86e-6	3.39e-5	-7.83e-5	1.18e-4	-1.08e-4	1.2e-5
e_1	-	-	3.61e-5	-5.28e-4	0.0032	-0.01	0.02	-0.023	0.015	-0.002
f_1	-	-	-0.0013	0.019	-0.114	0.371	-0.716	0.832	-0.537	0.036
g_1	-	-	-	-	-	-	-	0.299	3.874	0.231
a_2	-	3.64e-15	-5.84e-14	3.92e-13	-1.31e-12	2.18e-12	-1.12e-12	-1.48e-12	1.98e-12	-1.42e-13
b_2	-	-1.25e-12	2.01e-11	-1.26e-10	3.42e-10	-1.3e-10	-1.49e-9	3.48e-9	-2.8e-9	2.2e-10
c_2	-	-9.02e-10	1.49e-8	-1.05e-7	4.22e-7	-1.11e-6	2.02e-6	-2.38e-6	1.47e-6	-1.24e-7
d_2	-	4.89e-7	-8.05e-6	5.52e-5	-2.07e-4	4.74e-4	-7e-4	6.67e-4	-3.52e-4	3.08e-5
e_2	-	-6.69e-5	0.0011	-0.0075	0.028	-0.061	0.085	-0.074	0.036	-0.003
f_2	-	0.0017	-0.027	0.188	-0.702	1.572	-2.229	2.02	-1.025	0.075
g_2	-	-	-	-	-	-	-	0.397	4.046	0.086
a_3	-	1.54e-14	-2.48e-13	1.63e-12	-5.58e-12	1.04e-11	-1e-11	3.6e-12	5.35e-13	-1.54e-14
b_3	-	-1.5e-11	2.41e-10	-1.58e-9	5.35e-9	-9.85e-9	9.01e-9	-2.5e-9	-1.11e-9	7.07e-11
c_3	-	5.14e-9	-8.24e-8	5.35e-7	-1.79e-6	3.19e-6	-2.63e-6	2.63e-7	7.31e-7	-5.81e-8
d_3	-	-7.26e-7	1.15e-5	-7.39e-5	2.4e-4	-3.94e-4	2.39e-4	1.35e-4	-2.03e-4	1.77e-5
e_3	-	3.84e-5	-6e-4	0.004	-0.011	0.014	0.004	-0.029	0.023	-0.002
f_3	-	-9.57e-4	0.015	-0.088	0.242	0.219	-0.378	1.055	-0.778	0.055
g_3	-	-	-	-	-	-	-	0.513	4.275	0.213
a_4	-	3.53e-15	-6.56e-14	4.98e-13	-1.97e-12	4.31e-12	-4.91e-12	2.2e-12	3.09e-13	2.87e-14
b_4	-	-1.62e-12	3.47e-11	-2.92e-10	1.23e-9	-2.75e-9	2.93e-9	-6.79e-10	-9.51e-10	2.88e-11
c_4	-	-5.06e-10	5.15e-9	-1.33e-8	-1.78e-8	9.13e-8	9.61e-8	-6.42e-7	7.14e-7	-4.47e-8
d_4	-	3.65e-7	-5.46e-6	3.35e-5	-1.11e-4	2.28e-4	-3.27e-4	3.42e-4	-2.12e-4	1.61e-5
e_4	-	-5.39e-5	8.5e-4	-0.006	0.02	-0.041	0.056	-0.05	0.025	-0.002
f_4	-	0.002	-0.025	0.167	-0.608	1.336	-1.867	1.678	-0.847	0.051
g_4	-	-	-	-	-	-	-	0.394	4.041	0.362
a_5	-0.072	1.289	-9.732	40.46	-101	154.4	-141.3	72.53	-17.59	6.514
b_5	-	-0.048	0.814	-5.619	20.5	-42.47	49.82	-31.82	6.392	-1.234
c_5	-	-	-	-	-	-	-	0.477	2.799	1.619

Appendix 2: Maps of the differences between ΔE and $\Delta E_{\theta=0^\circ}$ (in canonical units-c.u.)

See Figs. 18, 19 and 20.

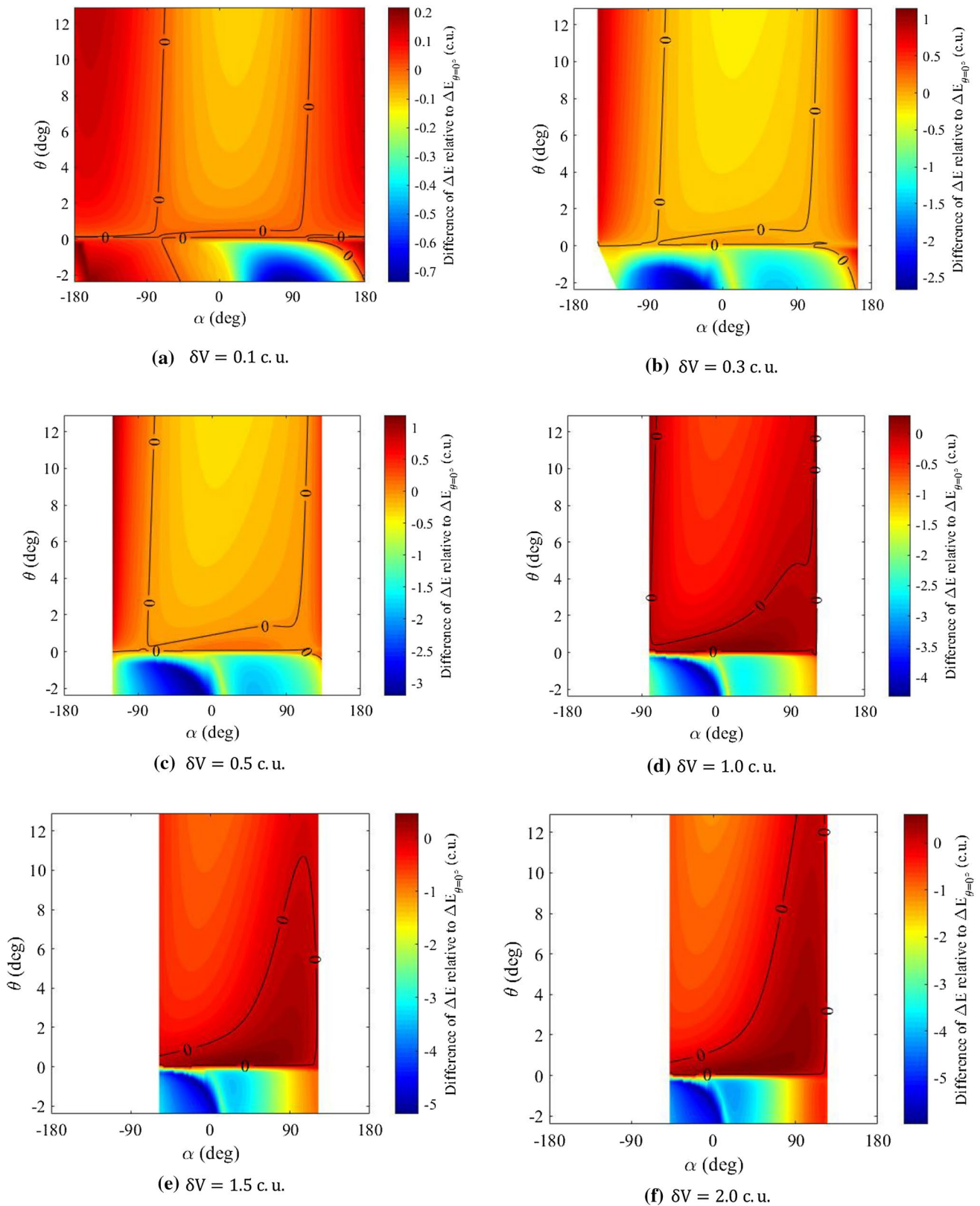


Fig. 18 Differences between the ΔE for free θ and ΔE for $\theta = 0^\circ$ (in canonical units—c.u.), for the situations where $e = 0.1, v = 0^\circ (t = 0), \psi = 270^\circ$ and δV goes from 0.1 to 2.0 c.u.

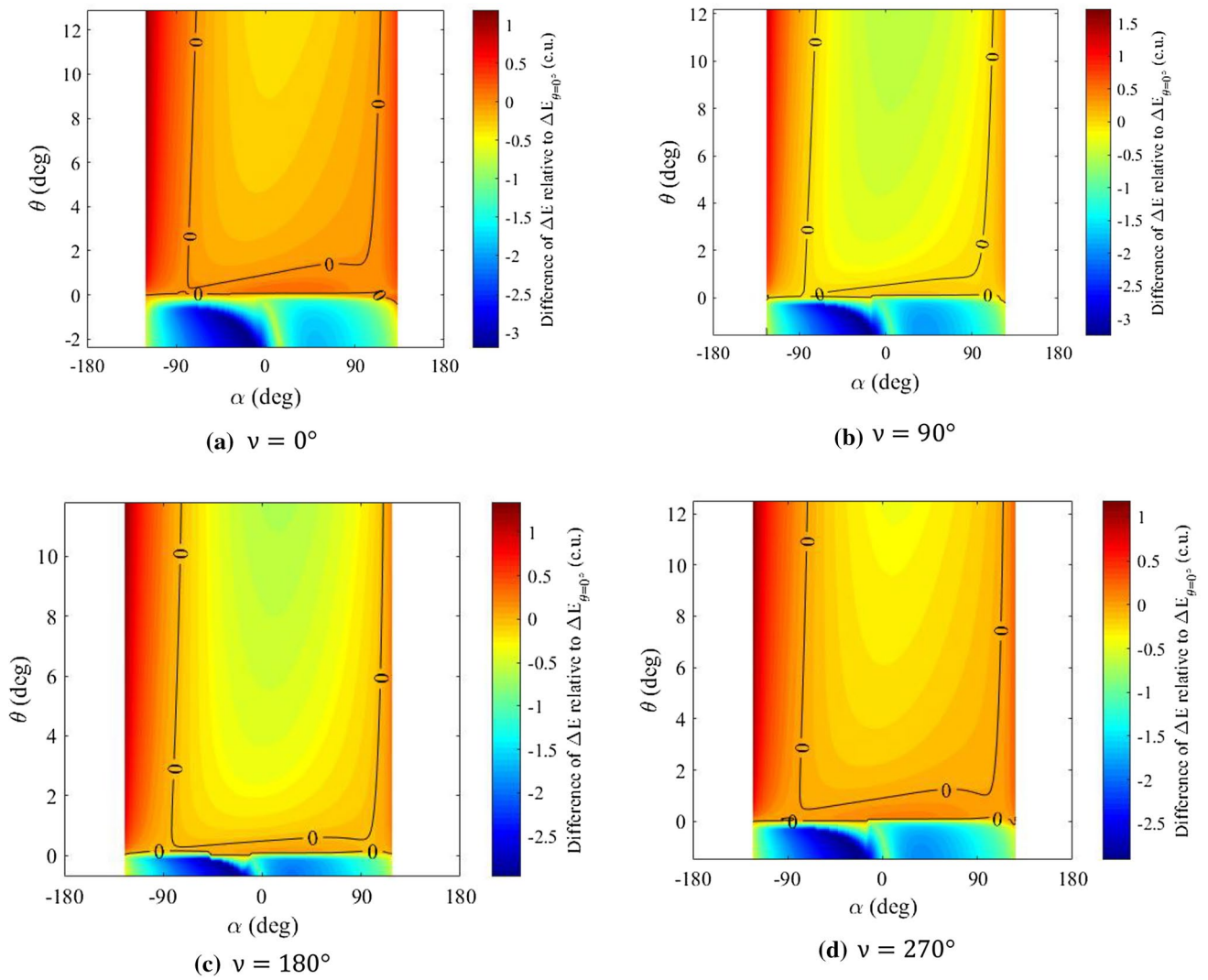


Fig. 19 Difference between the ΔE for free θ and ΔE for $\theta = 0^\circ$ (in canonical units—c.u.), for the situations where $e = 0.1$, $\psi = 270^\circ$, $\delta V = 0.5$ c.u. and different true anomalies

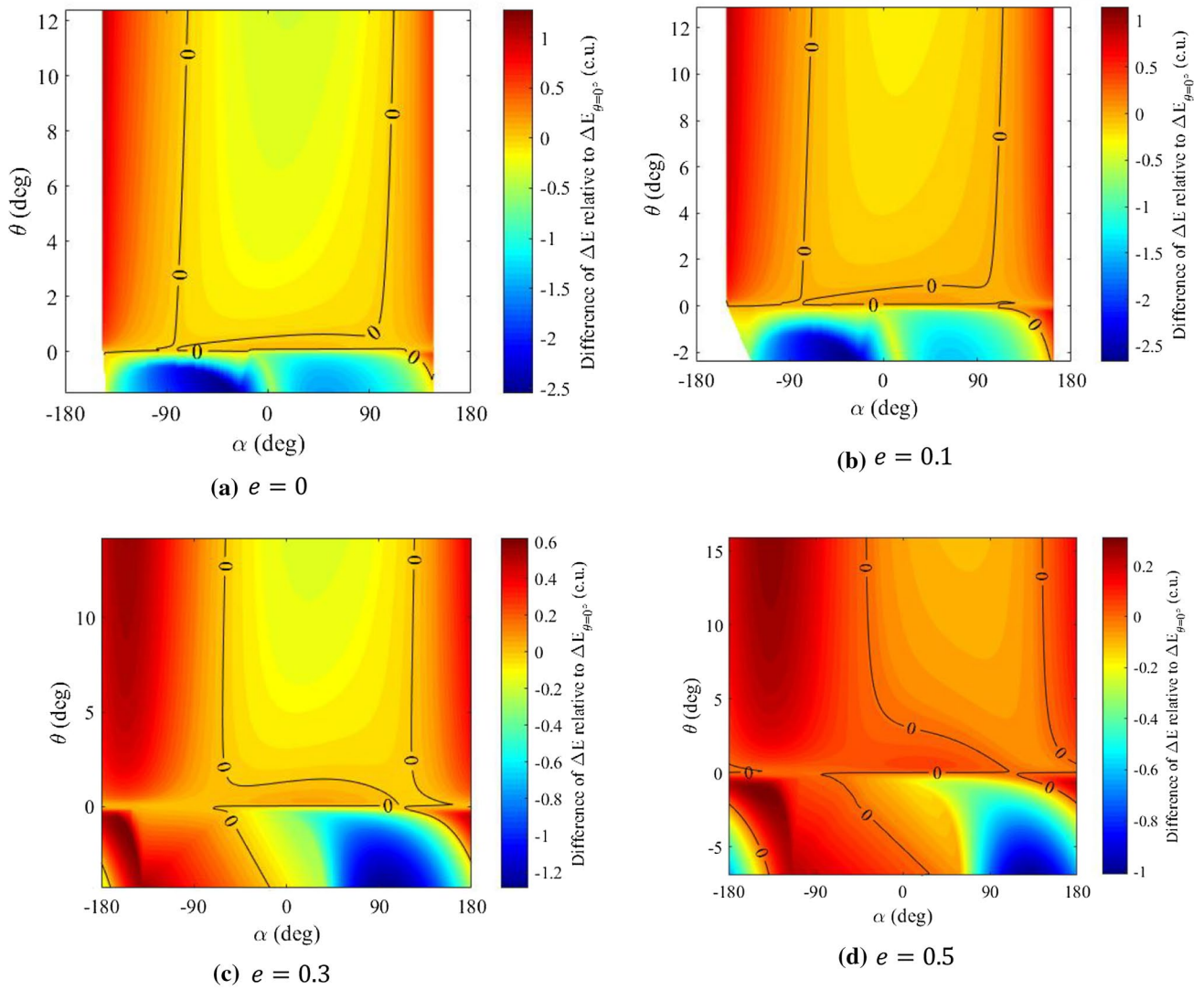


Fig. 20 Difference between the ΔE for free θ and ΔE for $\theta = 0^\circ$ (in canonical units—c.u.), for $\nu = 0^\circ (t = 0)$, $\psi = 270^\circ$, $\delta V = 0.3$ c.u. and different eccentricities

Acknowledgements The authors wish to express their appreciation for the support provided by Grants #305210/2018-1, 300923/2017-1, 406841/2016-0 and 301338/2016-7 from the National Council for Scientific and Technological Development (CNPq); Grants #2019/15180-0, 2016/24561-0 and 2016/23542-1 from São Paulo Research Foundation (FAPESP) and the financial support from the Coordination for the Improvement of Higher Education Personnel (CAPES).

Declaration

Conflict of interest The authors declare that they have no conflict of interest.

References

1. Minovitch MA (1961) A method for determining interplanetary free-fall reconnaissance trajectories. JPL, Pasadena. (JPL Tec. Memo 312-130)
2. Dowling RL, Kosmann WJ, Minovitch MA, Ridenoure RW (1990) The origin of gravity-propelled interplanetary space travel. In: Congress of the international astronomical federation, 41, 1990, Dresden, GDR. Proceedings... IAA, Dresden
3. Dowling RL, Kosmann WJ, Minovitch MA, Ridenoure RW (1991) Gravity propulsion research at UCLA and JPL 1962–1964. In: 41st Congress of the international astronomical federation, Dresden, GDR
4. Flandro GA (1966) Fast reconnaissance missions to the outer solar system utilizing energy derived from the gravitational field of Jupiter. *Astronaut Acta* 12(4):329–337
5. Damario LA, Byrnes DV, Stanford RH (1982) Interplanetary trajectory optimization with application to Galileo. *J Guid Control Dyn* 5:465–471. <https://doi.org/10.2514/3.56194>
6. Byrnes DV, D'Amario LA (1982) A combined Halley flyby Galileo mission. In: AIAA/AAS astrodynamics conference, San Diego, CA, AIAA paper 82-1462
7. McNutt RL, Solomon SC, Grard R, Novara M, Mukai T (2004) An international program for Mercury exploration: synergy of MESSENGER and BepiColombo. *Adv Space Res* 33(12):2126–2132. [https://doi.org/10.1016/S0273-1177\(03\)00439-3](https://doi.org/10.1016/S0273-1177(03)00439-3)
8. McNutt RL, Solomon SC, Gold RE, Leary JC (2006) The MESSENGER mission to Mercury: development history and early mission status. *Adv Space Res* 38(4):564–571. <https://doi.org/10.1016/j.asr.2005.05.044>
9. Grard R (2006) Mercury: the messenger and bepicolombo missions a concerted approach to the exploration of the planet. *Adv Space Res* 38(4):563
10. Greenberg R, Carusi A, Valsecchi GB (1988) Outcomes of planetary close encounters: a systematic comparison of methodologies. *Icarus*. [https://doi.org/10.1016/0019-1035\(88\)90125-X](https://doi.org/10.1016/0019-1035(88)90125-X)
11. Carusi A, Valsecchi GB, Greenberg R (1990) Planetary close encounters: geometry of approach and post-encounter orbital parameter. *Celest Mech Dyn Astron* 49(2):111–131
12. Campagnola S, Skerrett P, Russel RP (2012) Flybys in the planar, circular, restricted, three-body problem. *Celest Mech Dyn Astron* 113:343–368. <https://doi.org/10.1007/s10569-012-9427-x>
13. Gomes VM, Oliveira GMC, Prado AFBA, Sanchez DM (2016) Close approach of a cloud of particles around an oblate planet. *Comput Appl Math* 35:673. <https://doi.org/10.1007/s40314-015-0264-x>
14. Santana SHS, de Melo CF, Macau EEN (2016) Exploring the Moon gravity to escape from the Earth–Moon system. *Comput Appl Math* 35:701–710
15. Negri RB, Prado AFBA, Sukhanov AA (2017) Studying the errors in the estimation of the variation of energy by the “patched-conics” model in the three-dimensional swing-by. *Celest Mech Dyn Astron* 129:269–284. <https://doi.org/10.1007/s10569-017-9779-3>
16. Qi Y, de Ruiter A (2018) Energy analysis in the elliptic restricted three-body problem. *Mon Not R Astron Soc* 478:1392–1402. <https://doi.org/10.1093/mnras/sty1155>
17. Gagg Filho LA, Fernandes SS (2018) Interplanetary patched-conic approximation with an intermediary swing-by maneuver with the moon. *Comput Appl Math* 37:24–54
18. Broucke RA (1988) The celestial mechanics of gravity assist. In: AIAA/AAS astrodynamics conference, Minneapolis, MN, AIAA paper 88-4220 1988
19. Prado AFBA (1996) Powered Swing-By. *J Guid Control Dyn* 19:1142–1147
20. Casalino L, Colasurdo G, Pastrone D (1999) Optimal low-thrust escape trajectories using gravity assist. *J Guid Control Dyn* 22:637–642. <https://doi.org/10.2514/2.4451>
21. Casalino L, Colasurdo G, Pastrone D (1999) Simple strategy for powered Swing-By. *J Guid Control Dyn* 22:156–159
22. Ferreira AFS, Prado AFBA, Winter OC (2015) A numerical study of powered Swing-Bys around the Moon. *Adv Space Res* 56:252–272. <https://doi.org/10.1016/j.asr.2015.04.016>
23. Ferreira AFS, Prado AFBA, Winter OC (2017) A numerical mapping of energy gains in a powered Swing-By maneuver. *Nonlinear Dyn* 89:791–818. <https://doi.org/10.1007/s11071-017-3485-2>
24. Hollister WM, Prussing JE (1966) Optimum transfer to Mars via Venus. *Acta Astronaut* 12(2):169–179
25. Dunne J A, Burgess E (1978) The voyage of Mariner 10. National Aeronautics and Space Administration SP 424
26. Striepe SA, Braun RD (1991) Effects of a Venus Swing-By periaapsis burn during an Earth–Mars trajectory. *J Astronaut Sci* 39(3):299–312
27. Jehn R, Companys V, Corral C, Yáñez DG, Sánchez N (2008) Navigating BepiColombo during the weak-stability capture at Mercury. *Adv Space Res* 42(8):1364–1369
28. Ferreira AFS, Prado AFBA, Winter OC, Santos DPS (2017) Studying the energy variation in the powered Swing-By in the Sun-Mercury system. *J Phys Conf Ser* 911:012007. <https://doi.org/10.1088/1742-6596/911/1/012007>
29. Ferreira AFS, Prado AFBA, Winter OC, Santos DPS (2019) Effects of the mass parameter in the optimum direction of impulse and energy variation in a powered Swing-By. *J Phys Conf Ser* 1365:012008. <https://doi.org/10.1088/1742-6596/1365/1/012008>
30. Ferreira AFS, Prado AFBA, Winter OC, Santos DPS (2017) Effects of the eccentricity of the primaries in powered Swing-By maneuvers. *Adv Space Res* 59:2071–2087. <https://doi.org/10.1016/j.asr.2017.01.033>
31. Silva AF, Prado AFBA, Winter OC (2013) Powered swing-by Maneuvers around the Moon. *J Phys Conf Ser* 465:012001. <https://doi.org/10.1088/1742-6596/465/1/012001>
32. Szebehely V, Giacaglia GEO (1964) On the elliptic restricted problem of three bodies. *Astron J* 69:230. <https://doi.org/10.1086/109261>
33. Szebehely V (1967) *Theory of Orbits*. Academic Press, New York
34. Murray CD, Dermott SF (1999) *Solar system dynamics*, 1st edn. Cambridge University Press
35. Araujo RAN, Winter OC, Prado AFBA, Vieira MR (2008) Sphere of influence and Gravitational Capture radius: a dynamical approach. *Mon Not R Astron Soc* 391(2):675–684. <https://doi.org/10.1111/j.1365-2966.2008.13833.x>
36. Ferreira AFS, Prado AFBA, Winter OC, Santos DPS (2018) Analytical study of the powered Swing-By maneuver for

- elliptical systems and analysis of its efficiency. *Astrophys Space Sci* 363:145. <https://doi.org/10.1007/s10509-018-3362-6>
37. Ferreira AFS, Prado AFBA, Winter OC, Santos DPS (2018) Analytical study of the Swing-By maneuver in an elliptical system. *Astrophys Space Sci* 363:24. <https://doi.org/10.1007/s10509-017-3242-5>
38. Ferreira AFS, Prado AFBA, Winter OC (2018) Planar powered Swing-By maneuvers to brake a spacecraft. *Comput Appl Math* 37:202–219. <https://doi.org/10.1007/s40314-017-0483-4>

Publisher's Note Springer Nature remains neutral with regard to jurisdictional claims in published maps and institutional affiliations.